JOC The Journal of Organic Chemistry

Article

pubs.acs.org/joc

# Dumbbell-Type Fullerene-Steroid Hybrids: A Join Experimental and Theoretical Investigation for Conformational, Configurational, and Circular Dichroism Assignments

Alberto Ruíz,[†] Cercis Morera-Boado,[‡] Luis Almagro,[†] Julieta Coro,[†] Enrique E. Maroto,[§] María Ángeles Herranz,[§] Salvatore Filippone,[§] Dolores Molero,[∥] Roberto Martínez-Álvarez,[§] José M. Garcia de la Vega,[⊥] Margarita Suárez,*[,†] and Nazario Martín*[,§]

[†]Laboratorio de Síntesis Orgánica and [‡]Laboratorio de Química, Computacional y Teórica, Facultad de Química, Universidad de la Habana, 10400-La Habana, Cuba

[§]Departamento de Química Orgánica I and [∥]C.A.I. de Resonancia, Facultad de Ciencias Químicas, Universidad Complutense de Madrid, 28040-Madrid, Spain

[⊥]Departamento de Química Física Aplicada, Facultad de Ciencias, Universidad Autónoma de Madrid, 28049-Madrid, Spain

Supporting Information

**ABSTRACT:** New [60]fullerene-steroid conjugates (**4**–**6**) have been synthesized by 1,3-dipolar cycloaddition and Bingel–Hirsch cyclopropanation reactions from suitably functionalized epiandrosterone and [60]fullerene. Since a new stereocenter is created in the formation of the Prato monoaduct, two different diastereomers were isolated by HPLC (**4**, **5**) whose absolute configurations were assigned according to the highly reliable "sector rule" on fullerenes. A further reaction of the malonate-containing diastereomer **5** with a second $C_{60}$ molecule has afforded dumbbell fullerene **6** in which the two fullerene units are covalently connected through an epiandrosterone moiety. The new compounds have been spectroscopically characterized and their redox potentials, determined by cyclic voltametry, reveal three reversible reduction waves for hybrids **4** and **5**, whereas these signals are split in dumbbell **6**. Theoretical calculations at semiempirical (AM1) and single point B3LYP/6-31G(d) levels have predicted the most stable conformations for the hybrid compounds (**4**–**6**), showing the importance of the chlorine atom on the D ring of the steroid. Furthermore, TDDFT calculations have allowed assignments of the experimentally determined circular dichroism (CD) of the [60]fullerene-steroid hybrids based on the sign and position of the Cotton effects, despite the exceptionally large systems under study.

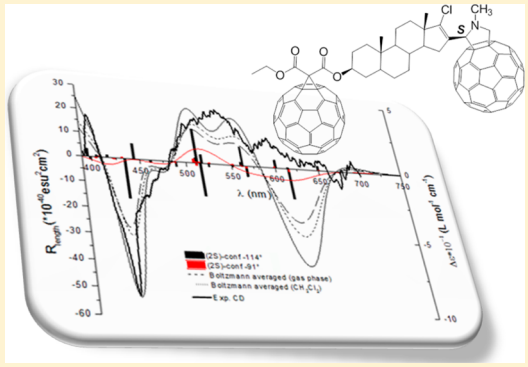


## INTRODUCTION

Soluble fullerene derivatives are essential for emerging biological and medical applications that exploit the unique chemical properties and spherical geometry of $C_{60}$.[1] In particular, fullerene-steroid hybrid systems are a very interesting family of compounds that has been investigated during the past decade due to the emerging of appealing features.[2] In particular, fullerenes have been covalently linked to steroids in order to decrease their hydrophobic character and to take advantage of the great variety of different biological functions that steroids display.

In fact, some of the reported hybrid systems based on steroid-[60]fullerenes have been synthesized mainly with the purpose of enhancing the therapeutic properties of fullerene itself. Knowing the ability of fullerenes to act as free-radical sponges[3] and to cause biochemical effects under the influence of light irradiation, some authors have studied their antioxidant capacity. As a representative example, Bjelakovic et al. have reported the antioxidant activity of fullero-steroid derivatives where the γ-aminobutyric acid (GABA) was incorporated to fulleropyrrolidine moieties. The resulting compounds showed an antioxidant activity 2–3 times larger than that of the parent fullerene.[4]

In the search for other different properties for medical use, fullerene-steroid conjugates have been prepared by Diels–Alder cycloaddition reaction. Preliminary studies revealed an effect of the synthesized compounds on sarcoplasmic reticulum (SR) $Ca^{2+}$-ATPase and survival of human lung adenocarcinoma cancer $A_{549}$ cells.[5] Other fullerene-steroid hybrids have also been synthesized using different linkers to attach the steroid moiety to $C_{60}$. Interestingly, it has been proved that the steroid moiety confers an adequate solubility in components of biological fluids.[6]

**Received:** January 28, 2014
**Published:** March 25, 2014

   dx.doi.org/10.1021/jo500178t | J. Org. Chem. 2014, 79, 3473–3486

**Scheme 1**[a]

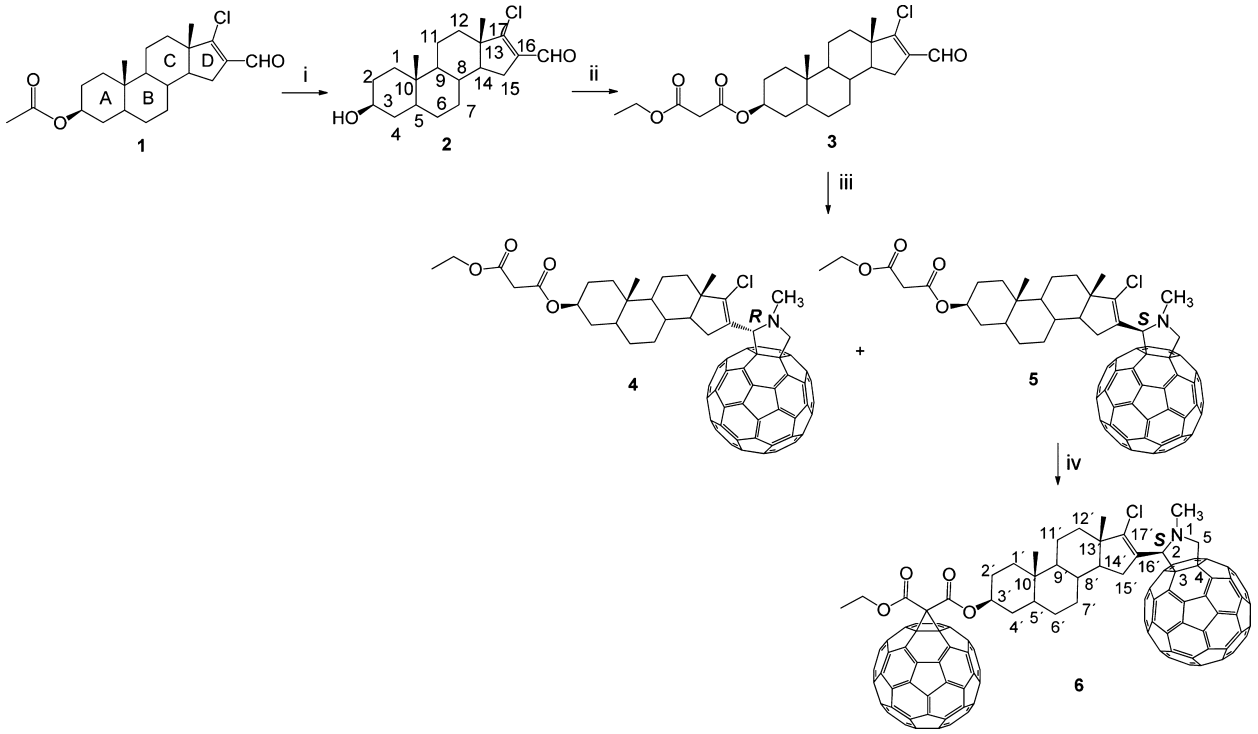


[a]Reagents and conditions: (i) $K_2CO_3$ (5%) MeOH, rt; (ii) (ethoxycarbonyl)acetyl chloride, DCM, pyridine, 0 °C; (iii) $C_{60}$, *N*-methylglycine, toluene, reflux; (iv) $C_{60}$, $CBr_4$, DBU, toluene, rt.

Besides the aforementioned properties, steroids have been used as templates for the construction of [60]fullerene-steroid bisadducts with controlled regio- and stereoselectivity.[7]

We have previously reported hybrid fullerene-steroid derivatives prepared by Bingel–Hirsch reaction by means of suitable malonates endowed with cholesterol, $\beta$-sitosterol, and ergosterol units.[8] More recently, a diastereoselective synthesis of $C_{60}$-steroid conjugates by Prato reaction has afforded a diasteromeric mixture of fulleropyrrolidine derivatives due to the generation of a new stereogenic center in the cyclization process.[9]

In this work we describe the multistep preparation of a fullerene hybrid dumbbell endowed with two fullerene units connected through an epiandrosterone molecule. Suitably functionalized epiandrosterone requires a previous chemical modification to introduce a formyl and a malonate group for further covalent connectivity to the $C_{60}$ units. In addition, we have investigated the experimental and theoretical chiroptical properties of the new dumbbell, which has allowed us to determine the absolute configuration of the new stereogenic center created during the cycloaddition process.

It is known that time dependent density funtional theory (TDDFT) simulations have emerged as a powerful tool for modeling the light absorption process of diverse chiral organic compounds, biomolecules, and metal complexes.[10] This method has allowed quantum mechanical calculation of the electronic circular dichroism spectra (ECD) and optical rotation dispersion at relatively low computational expense. The simulation of ECD by means of TDDFT is particularly useful in the assignment of the absolute configuration of chiral fullerenes[11−13] making it possible to understand the nature of the electronic transitions related to each Cotton effect (CE). In this sense, only a few studies have reported TDDFT methods to perform CD calculations on pristine fullerenes, namely, $C_{76}$, $C_{80}$, and $C_{84}$.[14] It has been recognized that the ECD spectra of inherently chiral fullerenes depend sensitively on the electronic structure and conformational changes.[15] Therefore, by means of TDDFT calculations, in this paper we have developed a conformational analysis of the synthesized compounds with the main goal to obtain the theoretical CD spectra and to properly assign the absolute configuration and electronic transitions of these complex fullerenes derivatives.

## RESULTS AND DISSCUSION

The synthesis of steroid-fullerene hybrids was carried out from the androsterone derivative **1** after several steps in which one and two molecules of $C_{60}$ have been joined to the steroid framework (see Scheme 1). Taking into account the well-stablished and efficient procedures available for the synthesis of fulleropyrrolidines[16] and methanofullerenes,[17] we choose these reactions with the purpose to obtain the fullerene hybrids in a straightforward manner. The presence of a formyl group at the C16 position of the D ring in **1** allows it to react with [60]fullerene through a 1,3-dipolar cycloaddition reaction. The second unit of $C_{60}$ was introduced by a cyclopropanation reaction following a previous transformation of the acetate group attached to the C3 position in ring A to the corresponding malonate (see Scheme 1).

The first step of the synthesis required the hydrolysis with potassium carbonate in methanol of the acetate group in C-3 position of the 3$\beta$-acetoxy-17-chloro-16-formyl-5$\alpha$-androstan-16-ene (**1**). The 17-chloro-16-formyl-3$\beta$-hydroxi-5$\alpha$-androstan-16-ene (**2**) was obtained in good yield (92%). The $^{13}$C NMR spectrum confirms the loss of the acetate group since the signal of carbonyl group present in **1** at 170.68 ppm[9] disappeared. Additionally, in the $^1$H NMR spectrum of **2** the signal of the


dx.doi.org/10.1021/jo500178t | J. Org. Chem. 2014, 79, 3473−3486

H3 proton of the steroid ring A is observed at $\delta$ = 3.61, which is shielded in relation to the same proton in steroid **1** (4.70 ppm).[9] The structure was further confirmed by elemental analysis and mass spectrometry. Under ESI-MS conditions compound **2** shows a peak corresponding to the sodiated molecule at $m/z$ = 359.1 $[M + Na]^+$ (see Experimental Section and Supporting Information).

The incorporation of the malonate moiety in steroid **3** was carried out from **2** by reaction with (ethoxycarbonyl)acetyl chloride in anhydrous dichloromethane and pyridine at 0 °C (Scheme 1). The new malonate **3** was obtained as a pale yellow solid after purification by flash chromatography with hexane/ethyl acetate (5:1) as eluent in a 82% yield. Compound **3** was fully characterized by the usual analytical and spectroscopic techniques (see Experimental Section and Supporting Information). For example, $^1$H NMR shows the signals corresponding to the steroid moiety and that assigned to the malonate fragment. In particular, it is worth mentioning that the signal corresponding to the H3 atom appears at 4.78 ppm, which is deshielded in comparison to the same proton in compound **2** and in a similar position to that in compound **1**. The methylene protons of the malonate fragment appear as a singlet at $\delta$ = 3.36. The $^{13}$C NMR spectrum shows signals at 166.7 and 166.1 ppm corresponding to the two carbonyl groups of the malonate moiety and another at 188.2 ppm assignable to the formyl group connected to C17. The structure was also confirmed by MS and elemental analysis. Under HRMS-MALDI-TOF conditions, the spectrum of **3** shows a peak corresponding to the sodiated molecule $[M + Na]^+$ at $m/z$ 473.2076 (see Experimental Section and Supporting Information).

Compound **3** bearing a formyl group allowed us to carry out the 1,3-dipolar cycloaddition by reaction with [60]fullerene and *N*-methylglycine in refluxing toluene to afford *N*-methyl-2-(3′$\beta$-ethylmalonate-17′-chloro-5′$\alpha$-androstan-16′-ene)pyrrolidine-[3,4:1,2][60]fullerenes **4** and **5**. The product of the Prato cycloaddition reaction contains a new stereocenter at C2 in the pyrrolidine ring, and therefore, two diastereomers are formed. These stereoisomers **4** and **5** are obtained in 55:45 ratio, respectively (HPLC), with moderate yields (**4**, 34%; **5**, 27%) as stable amorphous brown solids, which were easily separated by flash chromatography ($CS_2$, $CH_2Cl_2$, and $CH_2Cl_2$/hexane).

Both diasteroisomers **4** and **5** were thoroughly characterized using different spectroscopic techniques (see Experimental Section and Supporting Information). Besides the disappearance of the formyl proton (signal at $\delta$ ∼10 ppm) in the fulleropyrrolidines **4** and **5**, new signals corresponding to the protons of the pyrrolidine ring appear at $\delta$ 4.81 and 4.16 ppm as doublets ($J$ = 9.1 Hz; geminal protons) for compound **4** and as a broad signal at 4.89 and 4.18 ppm for compound **5**. The proton attached to the C2 of the pyrrolidine ring resonates at 5.01 and 5.04 ppm for **4** and **5**, respectively. The *N*-methyl protons appear at 2.75 (**4**) and 2.82 (**5**) ppm. The presence of the malonate moiety at position 3 of ring A is demonstrated by the signals assignable to the methylene group between the two esters at $\delta \approx$ 3.3 for both **4** and **5**, and the ethyl group at 1.29 ppm ($-CH_3$) and 4.22 ppm ($-CH_2-$) (**4**) and 1.28 ppm ($-CH_3$) and 4.21 ppm ($-CH_2-$) (**5**) with values of the coupling constant of ∼7 Hz. The remaining signals corresponding to the steroid protons are in agreement with the data reported for related compounds[9] (see Experimental Section).

The signals corresponding to the 6,6-ring junction of the $C_{60}$ cage can be clearly observed in the $^{13}$C NMR spectra of fulleropyrrolidines **4** and **5** at 75.51 and 69.82 ppm for compound **4** and 75.90 and 69.40 ppm for compound **5**. Also, the formation of the pyrrolidine ring could be verified by the presence of signals at 76.52 ppm (C2) and 69.62 ppm (C5) for compound **4** and 76.10 ppm and 69.93 ppm for diastereomer **5**. The methyl group attached to the nitrogen atom of the heterocyclic ring appears at 40.83 ppm for both diastereoisomers.

Also noteworthy are the signals present in the spectra of **4** and **5**, at 166.75 and 166.10 ppm, respectively, assignable to the carbonyl groups and the signal at ∼61 ppm corresponding to the methylene group of the malonate moiety. Additional NMR characterization was carried out by COSY, DEPT, HMQC, and HMBC experiments (see Suporting Information).

Mass spectrometry confirmed the structure of the synthesized compounds. The HRMS-MALDI-TOF spectrum for compound **4** shows a peak at 1198.2744 (calculated for $C_{87}H_{41}ClNO$ 1198.2724), corresponding to the protonated molecule $[M + H]^+$. Similarly, the HRMS-MALDI-TOF spectra of compound **5** shows a peak at 1198.2718, (calculated for $C_{87}H_{41}ClNO$ 1198.2724) also corresponding to $[M + H]^+$. Fragments at $m/z$ 477.9676 for **4** and at $m/z$ 478.0099 for **5** (calculated for $C_{27}H_{41}ClNO_4$ 478.2724), corresponding to the protonated ylide are observed. The formation of these fragments can be explained only by assuming a retro-cycloaddition reaction from the corresponding protonated molecules $[M + H]^+$. This process indicates that the protonation did not take place at the nitrogen atom of the pyrrolidine ring as we have previously reported.[18] The mass spectra of **4** and **5**, using negative mode of detection and DCTB [*trans*-2-[3-(4-*tert*-butylphenyl)-2-methyl-2-propenylidene]malononitrile] as matrix shows an odd-electron molecular ion at $m/z$ 1197 corresponding to $M^{\bullet-}$. In those cases the retro-cycloaddition process can be confirmed by the fragment at $m/z$ 720 (fullerene radical ion). The mass spectra relating to the above discussion are shown in the Supporting Information (Figures S14−S16, S21−S23).

Using diastereomer **5** as a representative compound, we carried out the reaction to obtain the fullerene dumbbell derivative **6** by connecting the malonate addend of **5** to [60]fullerene considering a cyclopropanation under Bingel−Hirsch conditions, treating **5** with $C_{60}$ in the presence of $CBr_4$ and DBU (see Scheme 1). After 4 h, the formation of the dumbbell derivative **6** was almost completed. Purification was achieved by flash chromatography, initially with carbon disulfide to elute unreacted $C_{60}$ and changing to a dichloromethane/hexane (4:1) mixture to obtain the pure fullerene dimer as a stable brown solid in 55% yield. The HPLC chromatograms of the reaction mixture (toluene/acetonitrile 9:1; 1 mL/min) showed **6** more retained (10.4 min) than the starting $C_{60}$ (8.9 min).

$^1$H NMR spectroscopy confirmed the formation of **6**. The signal corresponding to the protons of the methylene group between the two ester groups present in compound **5** (signal at 3.33 ppm), disappears and it is noteworthy that the signals corresponding to the protons of the ethoxycarbonyl group ($-CH_2-$ 4.48 ppm) are deshielded in comparison of those in compound **5** ($-CH_2-$ 4.21 ppm). The proton attached to the C2 of the pyrrolidine ring resonates 5.02 ppm, and those joined to C2 appear at $\delta$ 4.89 and 4.05 as broad signals. In addition, the signal of the proton on the C3 in ring A of the steroid is observed at 5.13 ppm, whereas in **5** it appears at 4.72 ppm. The rest of the signals corresponding to the steroid moiety and the


dx.doi.org/10.1021/jo500178t | J. Org. Chem. 2014, 79, 3473−3486

*N*-methyl protons do not differ significantly from those of the monoadduct **5** (see Experimental Section). On the other hand, as expected, in the $^{13}C$ NMR spectra the number of signals increases in the region where the carbons of the fullerenes cages appear. The $^{13}C$ NMR spectrum of **6** shows the presence of the two carbonyl groups at 164.02 and 163.50 ppm. The positions of the other steroid carbon atoms are very similar to those of compound **5**, the only exception being the C3 carbon atom in the steroid A rings, which are each deshielded by ca. 2 ppm, due to the presence of the new $C_{60}$ sphere. The signals of the carbons of the fulleropyrrolidine ring appear at 76.11 (C2) and 69.92 ppm (C5). In addition to the signals of the $C_{60}$ $sp^3$ carbons connected to the pyrrolidine ring at 75.92 and 69.73 ppm, the signals for the $sp^3$ carbon atoms of the $C_{60}$ connected to the cyclopropane ring in the dumbbell **6** appear at 71.22 and 74.30 ppm, whereas the signal of the quaternary carbon atom in the cyclopropane ring is observed at 50.12 ppm.

The HRMS-MALDI-TOF confirms the molecular formula of **6** showing a peak at *m*/*z* 1916.2642 (calculated for $C_{147}H_{39}ClNO_4$ 1916.2562) corresponding to $[M + H]^+$ (see Figure S28 in Supporting Information). Also, the MS-MALDI spectrum displays a peak at *m*/*z* 1938.2 due to $[M + Na]^+$ (see Figure S29 in Supporting Information).

According to the results observed for heterocyclic fused fullerenes and depending on the ionization conditions, either odd-electron molecular ions or even-electron protonated molecules can be detected.[17] Thus, compound **6** under MALDI ionization conditions shows a molecular ion $M^{\bullet-}$ at *m*/*z* 1915 using DCTB as matrix in negative mode of detection. Moreover, $[M + H]^+$ was observed at *m*/*z* 1916 when positive mode of detection was used (see Figures S30 and S31 in Supporting Information). The addition of NaI produces the formation of the corresponding $[M + Na]^+$ at *m*/*z* 1938 (see Figure S29 in Supporting Information).

The loss of 720 from $M^{\bullet+}$ as a consequence of the retro-cycloaddition reaction leads to the formation of a fragment at *m*/*z* 1195. The lack of fragments corresponding to fullerene $C_{60}$ indicates that the charge retention takes place at the ylide fragment (Figures S33 and S34 in Supporting Information).

Figure S36 in Supporting Information shows the UV−vis spectra of the fullerene-steroids hybrids **4**, **5**, and **6**, which show the typical profile of fullerene derivatives, all of them with a band centered at around 430 nm as a distinctive signature for fullerene monoadducts.

Cyclic voltammetry (CV) and Osteryoung square wave voltammetry (OSWV) were the techniques used to study the electrochemistry of steroids **4**−**6** in THF as solvent. Fulleropyrrolidine derivatives **4** and **5** exhibit three reduction waves, which are fully reversible in the solvent window investigated (Table 1). For the fullerene dimer **6** (Figure 1), the two fullerene species seem to behave independently, exhibiting the reduction potentials expected for the different addends connecting to the central core. The first reduction of both fullerenes units is observed as a broad signal centered at a $E^1_{1/2,red}$ = −0.95 V, whereas in the second reduction it is possible to distinguish the processes corresponding to the Bingel ($E^2_{1/2,red}$ = −1.48 V) or Prato ($E^2_{1/2,red}$ = −1.55 V) monoadducts. As previously observed by Cardullo and co-workers,[19] the nature of the fused addends has a significant influence on the first reduction potentials, and Bingel adducts are reduced more readily than fulleropyrrolidine adducts. The third reduction processes are shown independently and agree with the potential values observed in other methanofullerene[8] and fulleropyrrolidine (**4**, **5**) adducts.

**Table 1. Redox Potentials of Derivatives 4−6 and Reference $C_{60}$ vs Ferrocene in THF (V)**

| compd[a] | $E^1_{1/2,red}$ | $E^2_{1/2,red}$ | $E^3_{1/2,red}$ |
|---|---|---|---|
| $C_{60}$[b] | −0.86 | −1.44 | −2.00 |
| **4** | −1.00 | −1.57 | −2.20 |
| **5** | −0.99 | −1.55 | −2.18 |
| **6** | −0.95 (broad) | −1.48 | −2.04 |
| | | −1.55 | −2.20 |

[a]Experimental conditions: GCE as working electrode, Pt as counter electrode, $Ag/AgNO_3$ as reference electrode, $TBA{\cdot}PF_6$ (0.1 M) as supporting electrolyte, 100 mV/s scan rate. [b]Lerke, S. A.; Parkinson, B. A.; Evans, D. H.; Fagan, P. J. *J. Am. Chem. Soc.* **1992**, *114*, 7807−7813. The concentration of $TBA{\cdot}PF_6$ is 0.2 M.

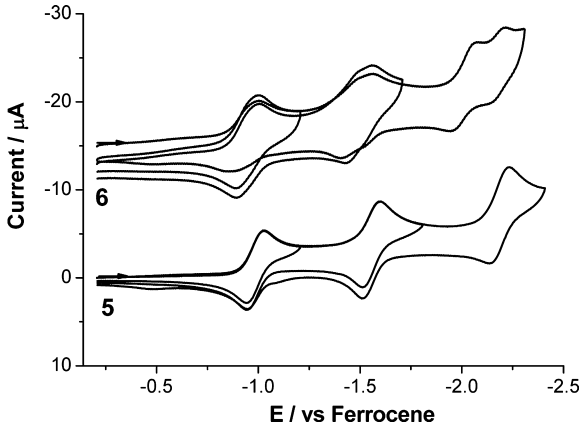


**Figure 1.** Cyclic voltammograms of compounds **5** and **6** in THF at room temperature.

The chiroptical properties of the new steroid-fullerene hybrids were investigated in a final step. Figure 2 shows the circular dichroism (CD) spectra of compounds **4** and **5**. Both diastereomers present CD spectra with contrary signs in the 430 nm region, pointing out the opposite absolute configurations at the C2 stereogenic center. This UV−vis band is considered to be the fingerprint for all monoadducts at 6,6 junctions, no matter what organic moiety saturates the double bond.

We have previously used[9,20−22] the sector rule proposed for fullerene derivatives, which allows determining the configuration of the new stereogenic center created in the reaction. This rule relates the Cotton effect (CE) associated with this UV−vis band and the stereochemical environment around the 6,6 junction. Compound **4** and **5** are CD-active, and by applying this rule, we have determined the absolute configuration of the C2 stereogenic carbon. Fulleropyrrolidine **4**, which exhibits a positive Cotton effect at 430 nm, (see Figure 2a) has a configuration of its sterogenic C2 center that can be assigned as *R*. On the other hand, compound **5**, whose CD spectrum shows a negative Cotton effect, has *S* configuration on the C2 (see Figure 2b). As expected, the CD spectrum of compound **6** (see Figure 2c) shows a negative Cotton effect because the chemical transformation of **5** to **6** does not involve any change in the stereogenic C2 atom, and the configuration of the C2 of compound **6** can be assigned as *S*. (for an exhaustive explanation see Figures S42−S45 in Supporting Information).


dx.doi.org/10.1021/jo500178t | *J. Org. Chem.* 2014, 79, 3473−3486

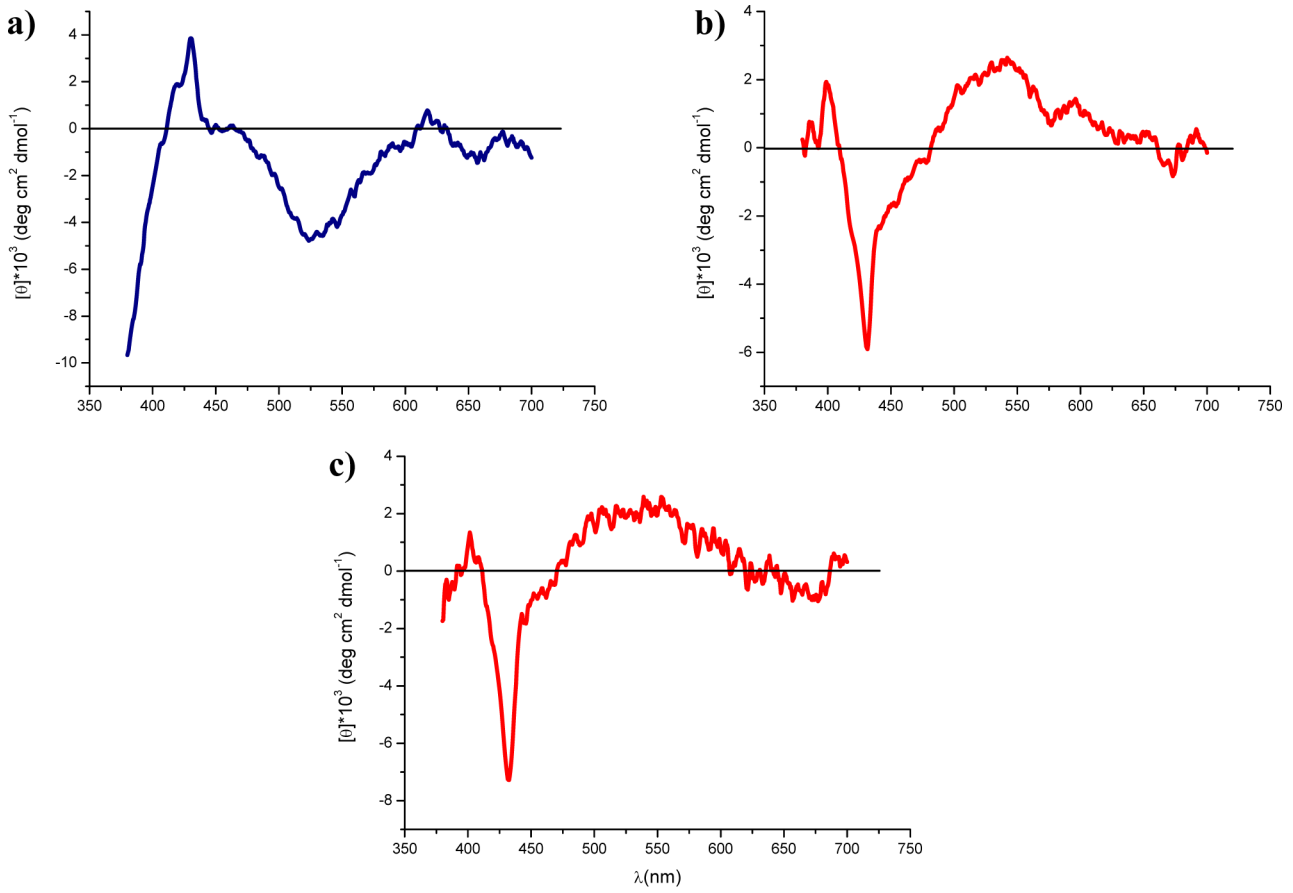


**Figure 2.** CD spectra of fulleroyrrolidines **4**–**6** (a–c) in $CH_2Cl_2$ ($4 \times 10^{-4}$ M).

For a better understanding of the geometrical and electronic properties of these molecules, we initially performed an AM1 conformational analysis[23] affording the minima energy conformations of compounds **4**-(2*R*), **5**-(2*S*), and **6**-(2*S*), presented in Figure 3. Other less stable configurations are shown in Figure S46 of Supporting Information.

The minima energy of **4**-(2*R*) and **5**-(2*S*) configurations show the stabilizing intramolecular C–H···Cl interaction that has been accepted as a very weak hydrogen bond, in the limit of van der Waals interactions.[24] These conformers represent the 37–48% of the whole population of each system, with distances $d_{H\cdots Cl}$, of 2.73–2.78 Å, which are considered as medium range C–H···Cl contacts.[25] These theoretical predictions are supported by experimental findings in the $^1$H NMR spectra. Thus, the methine proton on the C2 of the pyrrolidine ring appears typically at around 4.8–4.9 ppm.[26] However, the presence of a chlorine atom in the adjacent ring at the right distance to form a hydrogen bond results in a small but consistent downfield shift of the methine proton, which appears at 5.2–5.3 ppm.[9] In our case, this proton appears at 5.01–5.04 ppm, which is in agreement with the existence of a hydrogen bond. As expected, when chlorine and hydrogen atoms are in *trans* configuration, the conformers show a lower contribution to the partition functions of each system. These geometries show energetic destabilizations of 4.2 kcal/mol [**4**-(2*R*)], 5.3 kcal/mol [**5**-(2*S*)], and 4.3 kcal/mol [**6**-(2*S*)] with respect to the minima energy (obtained by B3LYP/6-31G(d)//AM1 level of calculation). Furthermore, it can be seen that the **4**-(2*R*) stereoisomer has shown C–H···Cl distances lower than the **5**-(2*S*) configuration, so it seems to be clear that this intramolecular C–H···Cl interaction contributes to the stabilization of the minima energy conformers. However, the calculated B3LYP/6-31G(d) energy differences between the most stabilized **4**-(2*R*) and **5**-(2*S*) conformers are low, about 1 kcal/mol.

It is important to note, however, that the energy difference calculated for the two rotamers, around 4 kcal/mol, is significantly lower than that required for the observation of both atropoisomers in solution.[9,27] In agreement with these calculated values, $^1$H NMR experiments in $CD_2Cl_2$ at low temperature (−60 °C) did not show the presence of any atropoisomer.

Figure 3 also reveals that although the preferred orientation of carbonyl groups in the C3-ethyl-malonate functionality is toward *trans* configuration, the dihedral angle defining the orientation of both C═O functionalities (O═C···C═O) can adopt different values and still show high stabilities. That is the case of the minima energy conformer of **5**-(2*S*) stereoisomer with a population of 47.7%, where the dihedral angle O═C···C═O is 64° and for **4**-(2*R*) the value is 156.3°, pointing out again that the most important stabilizing geometrical parameter of these molecules is the intramolecular C–H···Cl interaction. Then, as the disposition of the C3-ethyl-malonate group does not greatly affect the energy of these conformers (as proved by semiempirical AM1 and single point B3LYP/6-31G(d) energy calculations), an energy profile of the torsion angle C17′–C16′–C2–C3 at the B3LYP/6-31G(d) level of theory was performed to a model of compounds **4**-(2*R*) and **5**-(2*S*) without the C3-ethyl-malonate group. We expect that the removal of the C3-ethyl-malonate group does not affect the


dx.doi.org/10.1021/jo500178t | J. Org. Chem. 2014, 79, 3473–3486

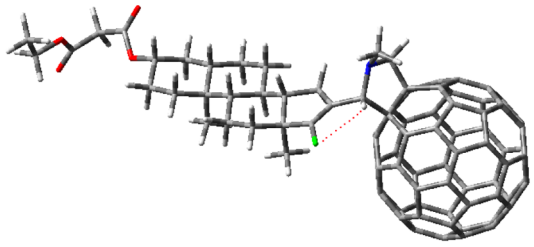

4-(2*R*)
(population 47.3%) dCl···H=2.73 Å, O=C···C=O = 156.3°

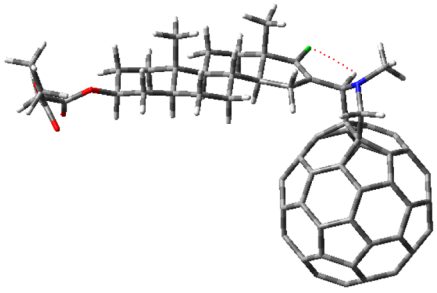

5-(2*S*)
(population 47.7%) dCl···H=2.78 Å, O=C···C=O = 64°

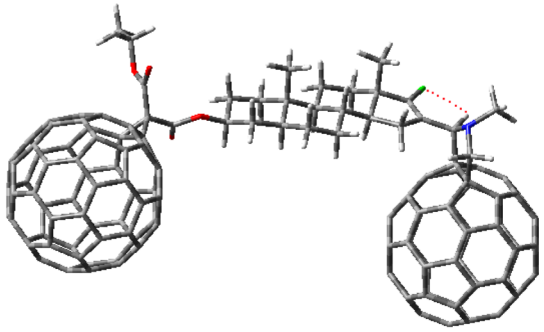

6-(2*S*)
(population 45.8%) dCl···H=2.77 Å, O=C···C=O = -159.4°

**Figure 3.** Minimum energy conformation (**4**–**6**) obtained by the AM1 method.

energy profile of these stereoisomers because, due to the stiffness of the entire molecule, the C17′−C16′−C2−C3 torsion angle is distant from the malonate functionality.

Figure 4 shows the energy profile of the models of diasteromers **4**-(2*R*) and **5**-(2*S*) without the C3-ethyl-malonate moiety. The energy barrier to transform A and B minima to A′ and B′ are, respectively, 4.2 and 3.6 kcal/mol. The **4**-(2*R*)-model stereoisomer conformer with the lowest energy shows a torsion angle C17′−C16′−C2−C3 of 98°, while for the **5**-(2*S*)-model stereoisomer the most important minimum was obtained for −91°. As expected, the most stable conformations obtained from both profiles show $d_{H\cdots Cl}$ in the range of 2.65−2.85 Å, while the maxima energy conformations show $d_{H\cdots Cl}$ greater than 3 Å. Although the **5**-(2*S*) model shows the lowest energy barrier, the difference with the **4**-(2*R*) is very small, less than 1 kcal/mol.

Tables S1 and S2 of Supporting Information show the relative energies, populations, and energy values (in hartrees) of each stereoisomer model, respectively. As can be seen for the **4**-(2*R*)-model, three conformers show the highest populations: **4**-(2*R*)-conf 98° (38.1%), **4**-(2*R*)-conf 108° (29.4%), and **4**-(2*R*)-conf 90°(23.5%). For the **5**-(2*S*)-model, only two conformers,

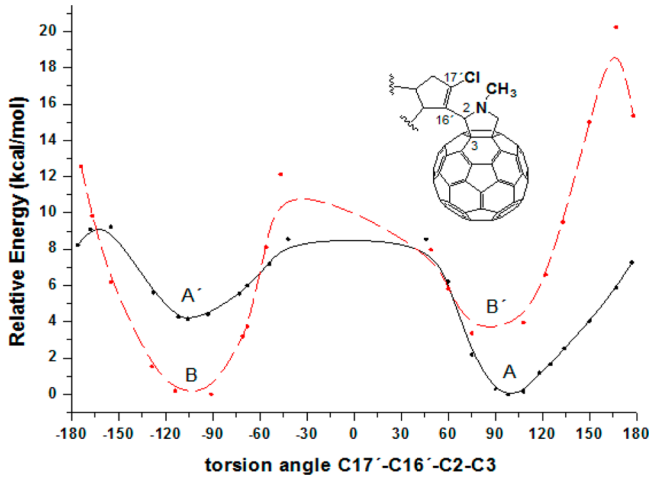


**Figure 4.** Rotational energy profile across the C17′−C16′−C2−C3 dihedral angle at the B3LYP/6-31G(d) level, for the **4**-(2*R*)-model (solid black line) and for the **5**-(2*S*)-model (red dashed line) configurations at C2.

**5**-(2*S*)-conf −91° (55.2%) and **5**-(2*S*)-conf −114° (40.1%) are the most important, with similar population contributions.

On the basis of the energy profile for the model of both diasteromer, we extended the minima energy geometries (**4**-(2*R*)-conf 98°, **4**-(2*R*)-conf 108°, **4**-(2*R*)-conf 90°, **5**-(2*S*)-conf −91°, and **5**-(2*S*)-conf −114°) by adding the C3-ethyl-malonate moiety in the same configuration as obtained by previous optimization of compounds **4**-(2*R*) and **5**-(2*S*) and calculated their circular dichroism spectra. Table 2 shows the relative energies $\Delta E$, $\Delta E_{ZPVE}$, and the conformer distributions taking into account both relative energies in the gas phase and with the effect of the $CH_2Cl_2$ solvent.

As can be seen from Table 2 and Table S1 in Supporting Information, the conformer distribution agrees well with those of the model used for obtaining the energy profile (Figure 4). The main difference is that, whereas **4**-(2*R*)-conf 98 and **5**-(2*S*)-conf −114° show the highest population (53.6% and 88.5%, respectively), for the geometries without the C3-ethyl-malonate group, similar populations were obtained for both model conformers (Table S1). The same behavior was observed for $\Delta E_{ZPVE}$ values, which provides **4**-(2*R*)-conf 98° and **5**-(2*S*)-conf −114° as the most important configurations of each conformer distribution.

To evaluate the effect of the $CH_2Cl_2$ solvent we employed the C-PCM model.[28−30] The geometries of the most stable minima (Table 2) have been reoptimized under the solution-phase CPCM condition. As can be seen, for both **4**-(2*R*) and **5**-(2*S*) conformers, the order of stabilities is maintained with respect to the gas-phase calculations, although the values are different. The lowest minima energy structures for **4**-(2*R*) and **5**-(2*S*) are **4**-(2*R*)-conf 98° and **5**-(2*S*)-conf −114°, respectively, but the geometries of **4**-(2*R*)-conf 108°, **4**-(2*R*)-conf 90°, and **5**-(2*S*)-conf −91° become more stable in solution than in the gas phase. The **4**-(2*R*)-conf 98° and **4**-(2*R*)-conf 108° in the solvent phase possess almost the same importance as reflected by $\Delta E$ (43.1% vs 30.9%) and $\Delta E_{ZPVE}$ (39.6% vs 34.8%) values, while in the gas phase a small difference in stabilities was obtained among **4**-(2*R*)-conf 108°and **4**-(2*R*)-conf 90° conformers. All of these data point out that the stability of individual conformers is clearly affected by the solvent. Subsequently, the calculated transitions, related


dx.doi.org/10.1021/jo500178t | J. Org. Chem. 2014, 79, 3473−3486

**Table 2. Relative Energies and Population Distribution of Most Stable Conformers of Stereoisomers 4-(2*R*), 5-(2*S*), and 6-(2*S*) at the B3LYP/6-31G(d) level of theory[a]**

| | conformer | $\Delta E^b$ | pop (%)[c] | $\Delta E_{ZPVE}{}^d$ | pop (%) |
|---|---|---|---|---|---|
| 4-(2*R*) | conf 90° | 0.62 (0.30) | 18.8 (26.0) | 0.27 (0.26) | 27.6 (25.6) |
| | conf 98° | 0 (0) | 53.6 (43.1) | 0 (0) | 43.7 (39.6) |
| | conf 108° | 0.39 (0.20) | 27.6 (30.9) | 0.25 (0.08) | 28.6 (34.8) |
| 5-(2*S*) | conf −91° | 1.21 (0.72) | 11.5 (23.0) | 0.86 (0.62) | 19.1 (26.0) |
| | conf −114° | 0 (0) | 88.5 (77.0) | 0 (0) | 80.9 (74.0) |
| 6-(2*S*) | conf −111° | 0 | 54.9 | 0 | 57.2 |
| | conf −109° | 0.117 | 45.1 | 0.171 | 42.8 |

[a]CPCM-B3LYP/6-31G(d) values are presented in parentheses only for 4-(2*R*) and 5-(2*S*). [b]Relative energy in kcal/mol. [c]Pop (%) conformational distribution calculated by using the respective parameters above at the B3LYP/6-31G(d). [d]Relative energy with ZPVE in kcal/mol.

rotatory strengths, and oscillator strengths of the major conformers of stereoisomers 4-(2*R*) and 5-(2*S*) are shown in Table S3 of Supporting Information in the gas and solvent phases.

The theoretical weighted and experimental CD curves of both diasteromers 4-(2*R*) and 5-(2*S*) are shown in Figure 5. The bars in Figure 5a and b represent the related scaled rotatory strengths by taking into account the conformer distribution and percentage populations obtained by the $\Delta E_{ZPVE}$ values in the gas and solvent phases. Although the $CH_2Cl_2$ solvent influences the relative stabilities of individual conformers, the shapes of the CD spectra of 4-(2*R*) and 5-(2*S*) are rather insensitive to the solvent effect. In general, the inclusion of the solvent effect does not improve the agreement between the experimental and averaged calculated spectra. For that reason, in the case of compound 6-(2*S*), as the stereogenic carbon shows the same stereochemistry (C-2*S*) that for 5-(2*S*) stereoisomer, we did not explore the changes with the $CH_2Cl_2$ solvent. In addition, as can be seen in Table S3 and Figure S47, both from Supporting Information, the position of the most important Cotton effects (CE) do not change significantly in solution respect to the gas phase. Therefore, in general, only the positions and nature of the transitions in the gas phase will be commented on and we will refer to the solvent effects in particular cases where small changes in CD curves respect to the gas phase were founded for particular conformers, e.g., the case of the 4-(2*R*)-conf 90° and 5-(2*S*)-conf −91°.

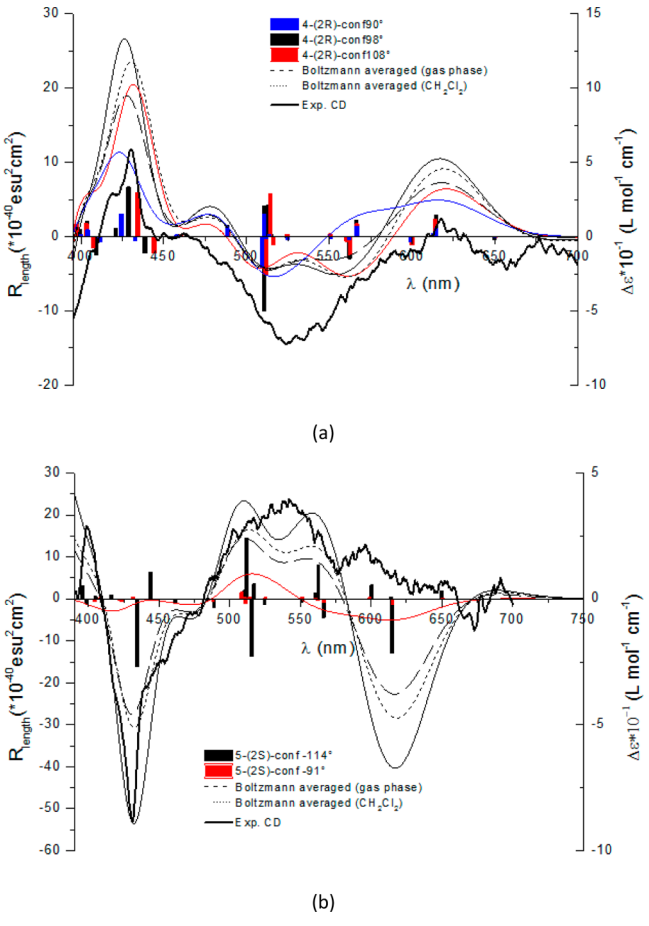


**Figure 5.** Calculated (at the B3LYP/6-31G(d) level) and experimental CD spectra of diasteromers (a) 4-(2*R*) and (b) 5-(2*S*). Percentage population of conformers: 4-(2*R*)-conf 90°; 4-(2*R*)-conf 98°; 4-(2*R*)-conf 108°; 5-(2*S*)-conf −114°; and 5-(2*S*)-conf −91° calculated on the basis of $\Delta E_{ZPVE}$ values for gas and $CH_2Cl_2$ solvent phases. Colored lines in each graph represent the individual conformers CD curves for each stereoisomer in correspondence with colored bars in the gas phase.

As shown in Figure 5 and Table S3 in Supporting Information, the calculated positive rotatory strength at 428.4, 434, and 424.1 nm of 4-(2*R*)-conf 98°, 4-(2*R*)-conf 108°, and 4-(2*R*)-conf 90°, respectively, may contribute to the experimentally observed high amplitude positive CE at 430 nm. On the other hand, only the 5-(2*S*)-conf −114° in the gas phase shows an intense negative rotatory strength at 434.3 nm, which contributes to the experimentally negative CE at 431 nm observed for this diastereoisomer. The less intense second broad band in the experimental spectra of both diasteromers includes several theoretical transitions in the range 510−570 nm, which show good agreement with the experimental CE centered at 525 nm for the 4-(2*R*) stereoisomer and at 543 nm for the 5-(2*S*) isomer. Overall, the basic patterns of the experimental CD curves of both diasteromers, e.g., sign and position of Cotton effects, are in agreement with TDDFT calculations in the gas and solvent phases. In both cases the most important CE found around 430 nm in the experimental CDs were reproduced by TDDFT/6-31G(d) calculations. The differences in the simulated gas-phase CD spectra of the two most stable conformers of 4-(2*R*), 4-(2*R*)-conf 98° and 4-(2*R*)-conf 108°, are quite small, while 4-(2*R*)-conf 90° exhibits a different behavior in the range of 550−600 nm (Figure 5a). A similar pattern was found for the 5-(2*S*) stereoisomer (Figure 5b), where the experimental CD spectrum was reproduced only by the 5-(2*S*)-conf −114° conformation in the gas phase. Thus, the CD spectra of the studied compounds in the gas phase are sensitive to changes of the dihedral C17′−C16′−C2−C3, where conformers with this torsion angle close to 90° for 4-(2*R*) or −90° for 5-(2*S*) do not reproduce the experimental


dx.doi.org/10.1021/jo500178t | J. Org. Chem. 2014, 79, 3473−3486

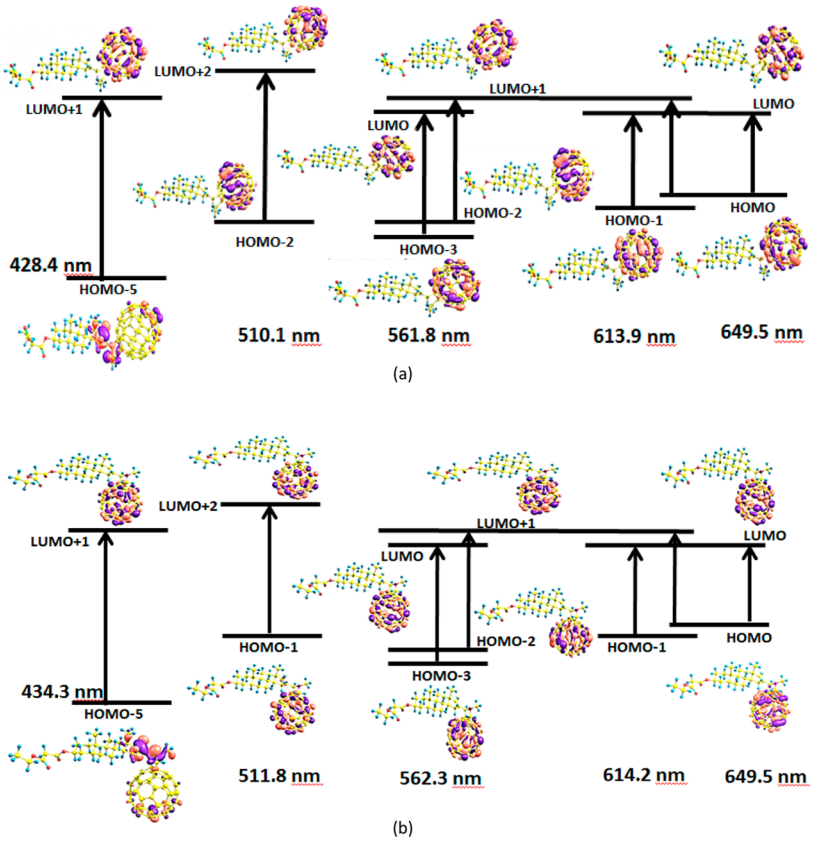


**Figure 6.** Molecular orbitals involved in the key transitions of CD in (a) **4**-(2*R*)-conf 98° and (b) **5**-(2*S*)-conf −114° of stereoisomers **4**-(2*R*) and **5**-(2*S*) at the B3LYP/6-31G(d) level of theory in the gas phase.

behavior. However, as noticed by Table S3 and Figure S47(e) of Supporting Information, the inclusion of the $CH_2Cl_2$ solvent in the CD spectrum of **5**-(2*S*)-conf −91° improves the description of the experimental negative CE around 431 nm with an increase in the rotational strength from $-3.1 \times 10^{-40}$ esu$^2$ cm$^2$ in the gas phase to $-9.4 \times 10^{-40}$ esu$^2$ cm$^2$ in the solvent phase. Also, for the reoptimized **4**-(2*R*)-conf 90° in the solvent phase, the most important positive CE (430 nm) shows greater rotational strengths as compared to gas-phase calculations, which therefore improves the description of the experimental CD by the inclusion of the solvent. In general, the solvent effect seems to be important only when the dihedral C17′−C16′−C2−C3 angle adopts perpendicular configurations [**4**-(2*R*)-conf 90° and **5**-(2*S*)-conf −91°], by increasing the rotational strengths of the first CE of both stereoisomers, although they are, however, much lower than the ones given by the other conformers for both diasteromers. This allow concluding that both experimental CD spectra are better reproduced by conformers where the C17′−C16′−C2−C3 torsion angle differs from 90° or −90° in both phases, e.g., 98° and 108° for **4**-(2*R*) and −114° for **5**-(2*S*).

Molecular orbitals (MO) involved in key transitions in the gas phase for the CD of the two major conformers of each diasteromer, e.g., **4**-(2*R*)-conf 98° and **5**-(2*S*)-conf −114°, are shown in Figure 6. Figure S48 from Supporting Information shows the key transitions in the solvent phase of these two conformers.

The major positive rotatory strength at 428.4 nm is contributed by the electronic transition from HOMO-5 to the LUMO+1 virtual orbital. The HOMO-5 occupied molecular orbital includes a delocalized $\pi$ bonding that involves $p_y$ and $p_z$ orbitals from carbon atoms of the double bond C17′═C16′ in ring D of the steroid, and the contribution of $p_y$ and $p_z$ orbitals from the chlorine atom and the lone pair from the nitrogen atom in the pyrrolidine ring. The same contributions were observed for the most negative rotatory strength at 434.3 nm of **5**-(2*S*)-conf −114°, Figure 6b. The same nature of transitions was found in the solvent phase as described in Table S3 and Figure S48 (Supporting Information).

The **4**-(2*R*)-conf 98° contributes to the second and less intense broad band of the experimental CD spectrum of **4**-(2*R*) with two negative rotatory strengths at 510 and 560 nm. The intense negative rotatory strength at 510.1 nm of **4**-(2*R*)-conf 98° may be attributed to the electronic transfer from HOMO-2, involving delocalized $\pi$ bonding orbitals of the C═C double bonds of the fullerene ring, to LUMO+2; this virtual unoccupied MO is also located in the fullerene moiety. The transition in 561.8 nm has the same nature than the previous one, but in this case the electronic transfer occurs primarily from HOMO-3 to LUMO (30%) and with a lower contribution from HOMO-2 to LUMO+1 (8%). The **5**-(2*S*)-conf −114° contributes to the second and less intense broad band of the experimental CD spectrum of diasteromer **5**-(2*S*) with three positive rotatory strengths at 511.8, 562.3, and 599.9 nm. These three theoretical transitions are related to electronic transfer that involve delocalized $\pi$ bonding orbitals of the C═C double bonds of the fullerene ring (HOMO-1, HOMO-3, and HOMO-2) to virtual $\pi^*$ unoccupied molecular orbitals also located in the fullerene moiety, i.e., LUMO+2 and LUMO, respectively. Although in the Boltzmann averaged spectra of **5**-(2*S*) there is an intense band around 614 nm with negative


dx.doi.org/10.1021/jo500178t | J. Org. Chem. 2014, 79, 3473−3486

rotatory strength that is absent in the experimental CD spectrum, this band is also present in the theoretical transitions of the three conformers of **4**-(2*R*) stereoisomer and with opposite rotatory strength sign. (Figure S49 from Supporting Information reveals that CD spectra of both diasteromers are oppositely signed curves in both gas and solvent phases.) In **4**-(2*R*) and **5**-(2*S*) compounds, these low energetic bands are mostly contributed by the electronic transition from HOMO to LUMO+1, which are again strong excitations from the $\pi$ delocalized orbitals of the fullerene into virtual $\pi^*$ orbitals of the same moiety (Figure 6a and b). The lowest energetic transition or first singlet excitation shows very low-amplitude negative and positive rotatory strengths for the **4**-(2*R*) and **5**-(2*S*), respectively. This can be attributed in both cases to the electronic $\pi-\pi^*$ transition between the HOMO and LUMO orbitals, showing the highest oscillator strengths (*f*). Taking into account that *f* is proportional to the squared of the electronic transition moment, it is reasonable to consider that this large *f* value is due to a strong charge delocalization through the whole fullerene functionality.

With the exception of HOMO-5, the other orbitals are dominated by the low lying $C_{60}$ orbitals. Although these low energy orbitals are usually symmetry forbidden (transitions in the range 560−615 nm), they are magnetically allowed, since the molecular orbitals occupied by the $\pi$ electrons are spherical as they reflect the shape of the fullerene.[31,32] As the intensity of a CD band, given by the rotational strength, is proportional to the imaginary part of the scalar product between the electronic and magnetic transition dipole moments,[33] then although several transitions are symmetry forbidden, they possess large magnetic moments that yield important CD signals. This is the case of several symmetry forbidden transitions with high rotational strengths found for all of the conformers of both diastereomers in the range 560−615 nm.

Overall, in the gas and solvent phases the nature of the most important positive [**4**-(2*R*)] and negative [**5**-(2*S*)] CE centered around 430 nm in the experimental CD spectra of both compounds can be attributed to $\pi-\pi^*$ and n$-\pi^*$ charge transfer transitions from the most important functionalities founded in the D (C═C and chlorine atom) and pyrrolidine (nitrogen atom) rings to the fullerene $\pi^*$ unoccupied orbitals. The nature of the other important transitions (515−650 nm) contributing to the second and less intense experimental band of these diasteromers are related ti $\pi-\pi^*$ transitions centered in the fullerene moiety. Our theoretical calculations show good agreement with experimental CD spectra.[34]

In addition, the calculation of the CD spectra of the dumbbell **6**-(2*S*) stereoisomer was obtained by means of the TDDFT-B3LYP/6-31G(d) level of theory. Figure 7 shows the comparison of the theoretical and experimental CD spectra of compound **6**-(2*S*).

Only in this case, the calculated spectra was blue-shifted by 0.850[35] to fit the position of the experimental CE around 432 nm. The bars in Figure 7 represent the related scaled rotatory strengths by having into account the conformer distribution and percentage populations obtained by the $\Delta E_{ZPVE}$ values at the B3LYP/6-31G(d) level of theory (Table 2). In this compound two major conformers, i.e., **6**-(2*S*)-conf −111° and **6**-(2*S*)-conf −109°, with similar populations (57.2% and 42.8%, respectively, according to $\Delta E_{ZPVE}$) were obtained after geometry optimization. It is interesting to note that after reoptimizing with DFT the minima energy obtained by the conformational analysis with the AM1 Hamiltonian method,

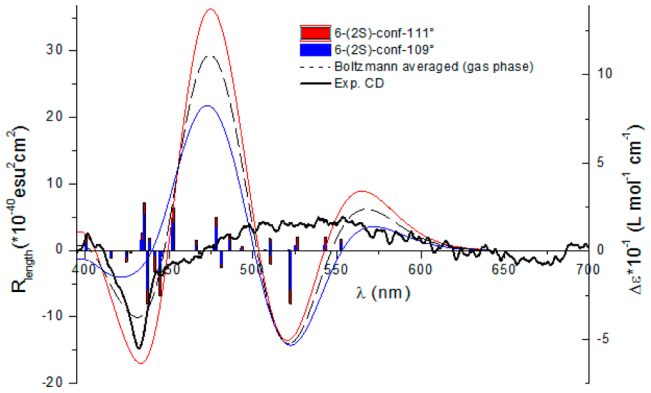


**Figure 7.** Calculated (at the B3LYP/6-31G(d) level) and experimental CD spectra of stereoisomer **6**-(2*S*). Percentage population of conformers: **6**-(2*S*)-conf −111, and **6**-(2*S*)-conf −109°, calculated on the basis of $\Delta E_{ZPVE}$ values.

the torsion C17′−C16′−C2−C3 angle for the two minima found [**6**-(2*S*)-conf −111° and **6**-(2*S*)-conf −109°] agrees quite well with the minima energy region for the similar **5**-(2*S*)-model compound (energy profile, Figure 4, B minimum). Although the agreement between the theoretical and experimental CD spectra is not as good as in the case of **4**-(2*R*) and **5**-(2*S*) fulleropyrrolidines, the main CE that characterizes the experimental spectrum of the **6**-(2*S*) compound, for instance, the negative CE at 432 nm, is well-represented by three transitions, i.e., 437.2, 441.5, and 444.7 nm for **6**-(2*S*)-conf −111° and 436.9, 441.7, and 444.7 nm in the case of the **6**-(2*S*)-conf −109° conformer. The second less intense experimental broad band with a positive experimental CE centered on 543 nm is mainly represented by the electronic transitions at 452.7, 486.4 nm [**6**-(2*S*)-conf −111°] and 452.2, 478.0 nm in the case of **6**-(2*S*)-conf −109°. Molecular orbitals (MO) involved in key transitions of the CD spectrum of the major conformer of **6**-(2*S*), i.e., **6**-(2*S*)-conf −111°, are shown in Figure 8. In addition, the calculated transitions, related rotatory strengths, and oscillator strengths of the major conformers of **6**-(2*S*) are shown in Table S4 and Figure S50 in Supporting Information.

The most important experimental negative CE is mainly contributed by three electronic transitions, where the HOMO-8 to LUMO shows the highest rotational strength. The nature of this transition is the same as the one observed for diasteromers **4**-(2*R*) and **5**-(2*S*) in Figure 6. Again, $\pi-\pi^*$ and n$-\pi^*$ charged transfer transitions occur among the chlorine atom, the C═C double bond in ring D, and the lone pair of the nitrogen atom in the pyrrolidine ring with unoccupied $\pi^*$ molecular orbitals centered in the fullerene moiety attached to the steroid D ring. The other two transitions involve $\pi-\pi^*$ transfer from HOMO-6 and HOMO-2 to the virtual orbital LUMO+4. It is interesting to note that these transitions involve charge transfer among $\pi$ occupied and virtual orbitals on the other fullerene functionality. Thus, it is expected for the dumbbell system **6**-(2*S*) to present a higher number of low lying orbital transitions as compared to the fulleropyrrolidines **4**-(2*R*) and **5**-(2*S*), which is caused by the existence of two [60]fullerenes molecules. Then, the second band with a positive CE centered at 475 nm involves also several electronic transitions of the same nature, namely, $\pi-\pi^*$ transitions from the same fullerene moiety, i.e., 452.7 and 486.4 nm [**6**-(2*S*)-conf −111°] or 452.2 and 478.0 [**6**-(2*S*)-conf −109°]; see Figure S50 in Supporting


dx.doi.org/10.1021/jo500178t | J. Org. Chem. 2014, 79, 3473−3486

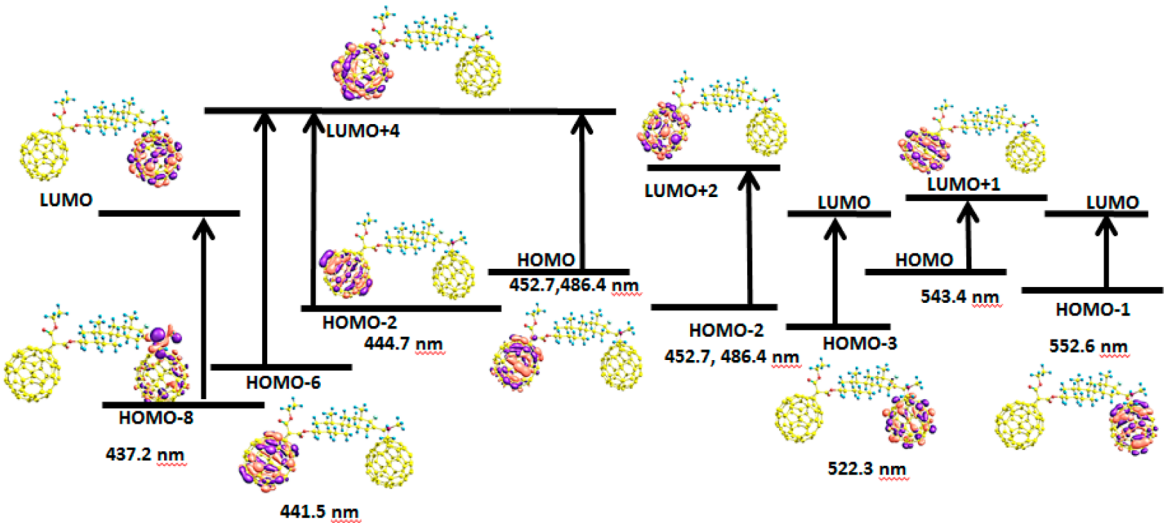


**Figure 8.** Molecular orbitals involved in the key transitions of CD in **6**-(2*S*)-conf −111° at the B3LYP/6-31G(d) level of theory.

Information. In addition, the other bands centered on 520 and 550 nm with negative and positive CE, respectively, for both conformers (Figure 6) show again transitions from highly delocalized occupied and virtual molecular orbitals centered in either of the fullerenes moieties. The conformer **6**-(2*S*)-conf −111°, with the highest stability, performs a better description of the most important experimental negative CE around 432 nm. Differences between the theoretical and experimental CD spectra could be related to the TDDFT method in this particular dumbbell compound.

As mentioned before, TDDFT possesses a well-known deficiency in cases where extended $\pi$-systems and charge transfer excitations of the molecules are important and the peak positions and intensities are affected.[34] In addition, the incompleteness of the basis set is also significant in the calculation of electronic spectra, where the use of diffuse functions seems to be essential. Thus, the existence of a high number of $\pi-\pi^*$ transitions and TDDFT failure in these extended $\pi$ systems could be the reason for the differences found among the theoretical and experimental CD in the case of the **6**-(2*S*) compound. Nevertheless, this is the first study that performs TDDFT on a large system involving two fullerene moieties, and the great value is that it makes it possible to comprehend the nature of the electronic transitions responsible for each of the bands presented in the experimental circular dichroism spectra.

## CONCLUSIONS

In summary, the synthesis of new [60]fullerene-steoids conjugates (**4**, **5**) prepared from suitably functionalized epiandrosterone by 1,3-dipolar cycloaddition of the steroid-containing azomethine ylide is described. HPLC separation of the two different diastereomer monoadducts formed has allowed the preparation of a new dumbbell molecule in which the second $C_{60}$ unit has been introduced by using the Bingel−Hirsh protocol. An exhaustive spectroscopic and electrochemical study has confirmed the proposed structures. In addition, we have carried out a thorough structural and electronic study at the semiempirical AM1 and single point B3LYP/631G(d) level of theory that has allowed the determineation of the most stable conformation for the obtained fullerene-steroids hybrids. Furthermore, the experimental circular dichroism (CD) spectra obtained for the different diastereomers (**4**, **5**) and dumbbell **6** have been assigned on the basis of the sign and position of the Cotton effects by TDDFT calculation in the gas and solvent phases, with a nice agreement. Interestingly, this is the first study in which TDDFT calculations have been used in large systems involving two $C_{60}$ units to reproduce the nature and electronic transitions observed in the CD spectra.

## EXPERIMENTAL SECTION

**General.** All reagents were of commercial quality and were used as supplied unless otherwise specified. Solvents were dried by standard procedures. All reactions were performed using an atmosphere of argon and oven-dried glassware. Reactions were monitored by thin-layer chromatography carried out on 0.25 mm silica gel plates (230−400 mesh). Flash column chromatography was performed using silica gel (60 Å, 32−63 $\mu$m). FTIR spectra were recorded in $CHCl_3$. $^1H$ NMR spectra were recorded at 700 MHz, and $^{13}C$ NMR at 175 MHz; the one-bond heteronuclear correlation (HMQC) and the long-range $^1H-^{13}C$ correlation (HMBC) spectra were obtained by use of the inv4gs and the inv4gslplrnd programs. All MASS-ESI and HRMS-MALDI (dithranol as matrix) experiments were carried out in negative and positive modes of detection. A high-performance liquid chromatography (HPLC) system (column dimensions, 4.6 mm × 250 mm; flow rate 1.0 mL/min, injection volume 15 $\mu$L, eluent toluene/acetonitrile 9:1) was used to determine the purity of the compounds synthesized. The retention times ($t_R$) reported were determined at a wavelength of 320 nm. Optical rotations were measured using a polarimeter with a thermally jacketed 10 cm cell at 25 °C (concentration given as g/100 mL). The CD spectra were recorded in $CH_2Cl_2$ (conc, $4 \times 10^{-4}$ M). High-performance liquid chromatography (column, 4.6 mm × 250 mm) was used to determine the purities of the compounds synthesized and the de values. The retention times ($t_R$) reported were determined at a wavelength of 320 nm. UV−vis spectra were recorded in $CHCl_3$.

**Theoretical Calculations.** A conformational analysis by using the semiempirical Hamiltonian AM1[23] through the Multiple Minima Hypersurfaces Methodology (MMH)[36] was initially carried out. This methodology performs a Monte Carlo simulation by randomly modifying the specified dihedral angles.[37] In this study, 200 conformations were created for each molecule, and the selected dihedrals were randomly generated for each conformation. We were interested in the conformational arrangement of two specific regions of these molecules, the linkage between the steroidal moiety and the fullerene and the disposition of both carbonyl functionalities in the


dx.doi.org/10.1021/jo500178t | J. Org. Chem. 2014, 79, 3473−3486

C3-ethyl-malonate group. Then, three dihedral angles were rotated for both **4**-(2*R*) and **5**-(2*S*) of each molecule, e.g., C21−O−C20−O, O−C18−O−C3, and C17′−C16′−C2−C3.

Single point energy calculations at the B3LYP/6-31G(d) level[38] were performed for the most important minima energy conformers. Also the lowest energy conformations found after AM1 conformational analysis of each stereoisomer were completely relaxed at the B3LYP/6-31G(d) level of theory; this was a time-consuming calculation. As a result of the conformational analysis performed with the AM1 semiempirical method, some AM1 geometries were reoptimized by using B3LYP/6-31G(d) with the goal to perform a DFT energy profile. AM1 geometries of the pyrrolidine-fullerenes **4**-(2*R*) and **5**-(2*S*) were simplified by a model of these compounds, e.g., the C3-ethyl-malonate functionality was removed from all geometries to be reoptimized. This change is justified in further explanations. In this reoptimization the dihedral C17′−C16′−C2−C3 was kept frozen at different values ranging from −180° to 180° in order to obtain an energy profile for both **4**-(2*R*) and **5**-(2*S*) models at the B3LYP/6-31G(d) level of theory. Frequency calculations were performed to ensure the presence of minima energy configurations.

The B3LYP/6-31G(d) energy profile was only obtained for compounds **4** and **5** since the compound **6** possess the same motive to be scanned (the heterocyclic ring motif attached to the steroid where the chirality is generated). In addition, the large size of compound **6** significantly increases the computational cost required to perform an energy profile for this molecule at the B3LYP/6-31G(d)level. Then, only the minima energy configurations obtained after the conformational AM1 analysis for compound **6** were reoptimized at the B3LYP/6-31G(d) level of theory.

Time dependent functional theory (TD-DFT)[39] calculations of the electronic circular dichroism spectra (CD) spectra were obtained for compounds **4**-(2*R*), **5**-(2*S*), and **6**-(2*S*) at the B3LYP/6-31G(d) level of theory. As the B3LYP/6-31G(d) energy profile was performed for a model of compounds **4** and **5**, where the molecules were calculated without the C3-ethyl-malonate group, in order to determine the CD spectra of the entire steroid-fullerene molecules, this group was added to each of the minima energy obtained from the B3LYP/6-31G(d) energy profile of both stereoisomer models. The C3-malonate group was added in the same configuration found after initial B3LYP/6-31G(d) optimization of both **4**-(2*R*) and **5**-(2*S*) diasteromers. The solvent effect with the implicit model conductor-like polarizable continuum model (C-PCM)[28−30] was employed to perform the ECD calculation of major conformers of **4**-(2*R*) and **5**-(2*S*) in $CH_2Cl_2$ solution at the B3LYP-CPCM/6-31G(d)//B3LYP/6-31G(d) level of theory. For the simulation of the CD spectra by TD-DFT, 50 vertical excitation energies $\Delta E_i$ and their rotational strength values $R_i$ were computed. To be able to compare theoretical and experimental CD data, the CD curve was simulated by using the Gaussian approximation.[40] Then, Gaussian functions with a full width at half-maximum (fwhm) of 20 nm were scaled to each of the calculated rotational strengths, which when summed approximated the experimental band shapes. For **4**-(2*R*) and **5**-(2*S*), percentage populations were calculated on the basis of $\Delta E$ and $\Delta E$ corrected with ZPVE values, using Boltzmann statistics at $T$ = 298 K. Due to their similarity, only $\Delta E_{ZPVE}$ values were taken for further considerations. Only in the case of **6**-(2*S*), the calculated spectrum at the B3LYP/6-31G(d) level of theory was blue-shifted by 0.850 to fit the position of the CE around 432 nm.

**Synthesis of Compounds.** *3β-Acetoxy-17-chloro-16-formyl-5α-androstan-16-ene (**1**).* This compound was prepared from 3β-acetoxy-5α-androstan-17-one by following the method previously reported in the literature in 68% yield (1.6 g), mp 131−132 °C (lit. 130−132 °C).[9]

*17-Chloro-16-formyl-3β-hydroxi-5α-androstan-16-ene (**2**).* To a stirred solution of 3β-acetoxy-17-chloro-16-formyl-5α-androstan-16-ene (**1**) (0.2 g, 0.53 mmol) in methanol (10 mL) was added an aqueous solution of $K_2CO_3$ (5%, 1.6 mL) dropwise, and then the reaction mixture was stirred for 24 h. Subsequently, the pH was adjusted to 3 with an aqueous HCl solution (1 N), and the mixture was stirred at room temperature for 1 h. Then, the solvent was removed *in vacuo*, and distillated water was added. The solid was filtered and washed several times with water. The product was isolated as a white solid, mp 123−124 °C, yield 0.16 g (0.48 mmol, 92%). $^1$H NMR (700 MHz, $CDCl_3$, 25 °C): δ 9.99 (s, 1 H, CHO), 3.61 (m, 1 H, 3-H), 2.54 (dd, $^3J_{HH}$ = 14.8 Hz, $J$ = 6.2 Hz, 1 H, 15-H), 2.05 (dd, $^3J_{HH}$ = 14.8 Hz, $^3J_{HH}$ = 4.3 Hz, 1 H, 15-H), 1.85 (m, 1 H, 12-H), 1.80 (m, 1 H, 2-H), 1.74 (m, 1 H, 7-H), 1.72 (m, 1 H, 1-H), 1.71 (m, 1 H, 11-H), 1.61 (m, 1 H, 8-H), 1.60 (m, 1 H, 4-H), 1.50 (m, 1 H, 14-H), 1.43 (m, 1 H, 12-H), 1.42 (m, 1 H, 2-H), 1.41 (m, 1 H, 11-H), 1.33 (m, 2 H, 6-H), 1.32 (m, 1 H, 4-H), 1.15 (tt, $^3J_{HH}$ = 12.5 Hz, $^3J_{HH}$ = 3.3 Hz, 1 H, 5-H), 1.01 (m, 1 H, 1-H), 0.97 (s, 3H, $CH_3$-13-C), 0.90 (m, 1 H, 7-H), 0.86 (s, 3 H, $CH_3$-10-C), 0.78 (m, 1 H, 9-H) ppm. $^{13}$C NMR (175 MHz, $CDCl_3$, 25 °C): δ 188.21 (CHO), 162.67 (C-17), 136.44 (C-16), 71.16 (C-3), 54.58 (C-9), 53.72 (C-14), 50.76 (C-13), 44.96 (C-5), 38.06 (C-4), 36.72 (C-1), 35.65 (C-10), 34.03 (C-8), 32.97 (C-12), 31.39 (C-2), 31.10 (C-7), 28.38 (C-6), 28.33 (C-15), 20.69 (C-11), 15.19 ($CH_3$-C-13), 12.28 ($CH_3$-C-10) ppm. IR ($CHCl_3$): ν 3339 (OH) 2924, 2854, 1732 (C═O), 1673, 1450, 1042 cm$^{-1}$. MS-ESI (MeOH): $[M + Na]^+$ $m/z$ for $C_{20}H_{29}ClNaO_2$ 359.1. Anal. Calcd for $C_{20}H_{29}ClO_2$: C, 71.30; H, 8.68. Found: C, 71.42; H, 8.55.

*17-Chloro-3β-ethyl Malonate-16-formyl-5α-androstan-16-ene (**3**).* A solution of 17-chloro-16-formyl-3β-hydroxi-5α-androstan-16-ene (**2**) (350 mg, 1.04 mmol) in anhydrous dichloromethane (25 mL) under argon was prepared. Pyridine (0.13 mL, 1.56 mmol) was added dropwise to the solution, and the resulting mixture was cooled with an ice bath. (Ethoxycarbonyl)acetyl chloride (0.2 mL, 1.56 mmol) was added dropwise. After stirring for 2 h, the solution was allowed to attain room temperature and stirred overnight. Water was then added, and the residue was extracted with $CH_2Cl_2$. The combined organic extracts were dried ($MgSO_4$) and filtered, and the solvent was removed under reduced pressure. Purification of products was achieved by column chromatography in silica gel with hexane/ethyl acetate (5:1) as eluent. The product was obtained as a pale yellow solid, yield 343 mg (0.76 mmol, 82%) mp 52−54 °C. $^1$H NMR (700 MHz, $CDCl_3$, 25 °C): δ 10.00 (s, 1 H, CHO), 4.78 (m, 1 H, 3-H), 4.22 (q, $^3J_{HH}$ = 7.1 Hz, 2 H, $CH_2$), 3.36 (s, 2 H, $CH_2$), 2.55 (dd, $^3J_{HH}$ = 14.7 Hz, $J$ = 7.0 Hz, 1 H, 15-H), 2.05 (dd, $^3J_{HH}$ = 14.7 Hz, $^3J_{HH}$ = 11.7 Hz, 1 H, 15-H), 1.88 (m, 1 H, 2-H), 1.85 (m, 1 H, 12-H), 1.74 (m, 1 H, 7-H), 1.75 (m, 1 H, 1-H), 1.71 (m, 1 H, 11-H), 1.61 (m, 1 H, 4-H), 1.60 (m, 1 H, 8-H), 1.53 (m, 1 H, 2-H), 1.51 (m, 1 H, 14-H), 1.42 (m, 1 H, 12-H), 1.41 (m, 1 H, 11-H), 1.37 (m, 1 H, 4-H), 1.35 (m, 2 H, 6-H), 1.30 (t, $^3J_{HH}$ = 7.1 Hz, 3 H, $CH_3$), 1.22 (tt $^3J_{HH}$ = 12.4 Hz, $^3J_{HH}$ = 3.1 Hz 1 H, 5-H), 1.06 (m, 1 H, 1-H), 0.98 (s, 3 H, $CH_3$-13-C), 0.90 (m, 1 H, 7-H), 0.87 (s, 3 H, $CH_3$-10-C), 0.80 (m, 1 H, 9-H). $^{13}$C NMR (175 MHz, $CDCl_3$, 25 °C): δ 188.18 (CHO), 166.74 (C═O), 166.17 (C═O), 162.53 (C-17), 136.44 (C-16), 74.71 (C-3), 61.45 ($CH_2$), 54.36 (C-9), 53.58 (C-14), 50.77 (C-13), 44.71 (C-5), 41.97 ($COCH_2CO$), 36.37 (C-1), 35.67 (C-10), 33.96 (C-8), 33.62 (C-4), 32.87 (C-12), 30.96 (C-7), 28.34 (C-6), 28.14 (C-15), 27.15 (C-2), 20.61 (C-11), 15.15 ($CH_3$-C-13), 14.07 ($CH_3$), 12.14 ($CH_3$-C-10). IR ($CHCl_3$): ν 2929, 2857, 2726, 1739 (C═O), 1673 (C═O), 1305, 1020 cm$^{-1}$. HRMS-MALDI-TOF: $[M + Na]^+$ $m/z$ calcd for $C_{25}H_{35}ClNaO_5$ 473.2065, found 473.2076. Anal. Calcd for $C_{25}H_{35}ClO_5$: C, 66.58; H, 7.82. Found: C, 66.51; H, 7.79.

*Synthesis of N-Methyl-2-(3′β-ethylmalonate-17′-chloro-5′α-androstan-16′-ene)pyrrolidino[3,4:1,2][60]fullerenes.* A mixture of $C_{60}$ (168 mg, 0.15 mmol), *N*-methylglycine (100 mg, 1.15 mmol), and the chloroformyl steroid **3** (120 mg, 0.27 mmol) in toluene (250 mL) under argon atmosphere was heated at reflux for 5 h. The color of the solution changed from purple to brown. The solvent was removed under reduced pressure, and the solid residue thus obtained was purified by column chromatography on silica gel, using $CS_2$ to elute unreacted $C_{60}$ and dichloromethane or dichlorometane/hexane (specified below for each compound **4** and **5**) to elute the corresponding pyrrolidino[3,4:1,2][60]fullerene. Additional purification of these compounds was carried out by repetitive precipitation and centrifugation using hexane, methanol, and diethyl ether as solvents.

*N-Methyl-(2R)-(3′β-ethylmalonate-17′-chloro-5α-androstan-16′-ene)pyrrolidino[3,4:1,2][60]fullerene (**4**).* The purification was


dx.doi.org/10.1021/jo500178t | J. Org. Chem. 2014, 79, 3473−3486

performed by column chromatography on silica gel with $CS_2$ and dichloromethane/hexane (4:1) as eluents, yield 100 mg (0.050 mmol, 34%), amorphous brown solid. HPLC: toluene/acetonitrile (95:5), flow rate 1 mL/min, $t_R$ = 7.19 min. $[\alpha]^{20}_D$ = +90 ($c$, 2 × $10^{-4}$ $CH_2Cl_2$). $^1$H NMR (700 MHz, $CDCl_3$, 25 °C): $\delta$ 5.01 (s, 1 H, 2-H), 4.81 (d, $^3J_{HH}$ = 9.1 Hz, 1 H, 5-H), 4.79 (m, 1 H, 3′-H), 4.22 (q, $J$ = 7.1 Hz, 2 H, $CH_2$), 4.16 (d, $J$ = 9.1 Hz, 1 H, 5-H), 3.35 (s, 2 H, $CH_2$), 2.75 (s, 3 H, $CH_3$-N), 2.82 (m, 1 H,15′-H), 2.14 (dd, $^3J_{HH}$ = 14.6 Hz, $^3J_{HH}$ = 11.5 Hz, 1 H, 15′-H), 1.88 (m, 1 H, 2′-H), 1.82 (m, 2 H, H7′, 12′-H), 1.75 (dt, $^3J_{HH}$ = 12.9 Hz, $^3J_{HH}$ = 3.4 Hz, 1 H, 1′-H), 1.55 (m, 1 H, 8′-H), 1.67 (m, 1 H, 4′-H), 1.68 (m, 1 H, 11′-H), 1.53 (m, 1 H, 2′-H), 1.39 (m, 1 H, 4′-H), 1.37 (m, 1 H, 11′-H), 1.66 (m, 1 H, 14′-H), 1.44 (m, 1 H, 12′-H), 1.29 (t, $^3J_{HH}$ = 7.1 Hz, 3 H, $CH_3$), 1.28 (m, 2 H, 6′-H), 1.15 (m, 1 H, 5′-H), 1.09 (m, 1 H, 7′-H),1.07 (td, $^3J_{HH}$ = 12.9 Hz, $^3J_{HH}$ = 3.4 Hz, 1 H, 1′-H), 0.83 (s, 3 H, $CH_3$-C-10′), 0.80 (m, 1 H, 9′-H), 0.75 (s, 3 H, $CH_3$-C-13′). $^{13}$C NMR (175 MHz, $CDCl_3$, 25 °C): $\delta$ 166.75 (C═O), 166.22 (C═O), 156.04, 154.30, 154.07, 153.32, 147.43, 147.28 (C-17), 146.52, 146.34, 146.29, 146.26, 146.19, 146.17, 146.08, 146.05, 146.02, 145.99, 145.74, 145.60, 145.49, 145.47, 145.43, 145.36, 145.31, 145.21, 145.16, 144.73, 144.67, 144.52, 144.41, 144.34, 143.13, 143.02, 142.66, 142.63, 142.58, 142.24, 142.20, 142.17, 142.08, 142.00, 141.92, 141.86, 141.80, 140.26, 140.06, 140.03, 139.44, 137.26, 136.83, 135.31, 135.76, 135.40, 133.26 (C16′), 76.52 (C2), 75.51 ($Csp^3$-$C_{60}$), 74.84 (C-3′), 69.82 ($Csp^3$-$C_{60}$), 69.62 (C-5), 61.45 ($CH_2$), 55.55 (C-14′), 54.68 (C-9′), 49.09 (C-13′), 44.85 (C-5′), 41.99 ($CH_2$), 40.83 ($CH_3$-N), 36.45 (C-1′), 35.74 (C-10′), 33.69 (C-12′), 33.99 (C-8′), 33.57 (C-4′), 32.05 (C-15′), 31.24 (C-7′), 28.69 (C-6′), 27.20 (C-2′), 20.75 (C-11′), 16.04 ($CH_3$-C-13′), 14.08 ($CH_3$), 12.17 ($CH_3$-C-10′). IR ($CHCl_3$): $\nu$ 2928, 2855, 2783, 1739, 1221, 1025, 772 $cm^{-1}$. UV−vis: $\lambda_{max}$ (log $\varepsilon$) 434 (3.70), 326 (4.60), 310 (4.55) nm. HRMS-MALDI-TOF: $[M + H]^+$ $m/z$ calcd for $C_{87}H_{41}ClNO_4$ 1198.2724, found 1198.2744.

*N-Methyl-(2S)-(3′β-ethylmalonate-17′-chloro-5α-androstan-16′-ene)pyrrolidino[3,4:1,2][60]fullerene (**5**).* The purification was performed by column chromatography on silica gel with $CS_2$ and dichloromethane as eluents, yield 80 mg (0.067 mmol, 27%), amorphous brown solid. HPLC: toluene/acetonitrile (95:5), flow rate 1 mL/min, $t_R$ = 8.19 min. $[\alpha]^{20}_D$ = +27.5 ($c$, 2 × $10^{-4}$ $CH_2Cl_2$). $^1$H NMR (700 MHz, $CDCl_3$, 25 °C): $\delta$ 5.04 (br s, 1 H, 2-H), 4.89 (br s, 1 H, 5-H), 4.72 (m, 1 H, 3′-H), 4.21 (q, $^3J_{HH}$ = 14.3 Hz, $^3J_{HH}$ = 7.2 Hz, 2 H, $CH_2$), 4.18 (br s, 1 H, 5-H), 3.33 (s, 2 H, $CH_2$), 2.82 (s, 3 H, $CH_3$-N), 2.79 (m, 1 H, 15′-H), 2.42 (m, 1 H, 15′-H), 1.83 (m, 1 H, 2′-H), 1.77 (m, 1 H, 12′-H), 1.73 (m, 1 H, 7′-H), 1.69 (dt, $^3J_{HH}$ = 13.7 Hz, $^3J_{HH}$ = 3.7 Hz, 1 H, 1′-H), 1.61 (m, 1 H, 4′-H), 1.60 (m, 1 H, 8′-H), 1.59 (m, 1 H, 11′-H), 1.50 (qd $^3J_{HH}$ = 12.9 Hz, $^3J_{HH}$ = 3.0 Hz, 1 H, 2′-H), 1.37 (m, 1 H, 4′-H), 1.36 (m, 1 H, 11′-H), 1.29 (m, 1 H, 14′-H), 1.28 (t, $^3J_{HH}$ = 7.2 Hz, 3 H, $CH_3$), 1.20 (m, 3 H, 6′-H, 12′-H), 1.16 (m, 1 H, 5′-H), 1.07 (s, 3 H, $CH_3$-C-13′), 1.04 (td, $^3J_{HH}$ = 13.7 Hz, $^3J_{HH}$ = 3.7 Hz, 1 H, 1′-H), 0.86 (s, 3 H, $CH_3$-C-10′), 0.75 (m, 1 H, 7′-H), 0.67 (m, 1 H, 9′-H). $^{13}$C NMR (175 MHz, $CDCl_3$, 25 °C): $\delta$ 166.73 (C═O), 166.10 (C═O), 156.07, 154.09, 153.91, 152.84, 147.33, 147.28, 146.68 146.55 (C17′), 146.39, 146.30, 146.19, 146.09, 146.05, 146.01, 145.97, 145.77, 145.56, 145.49, 145.44, 145.39, 145.37, 145.35, 145.30, 145.25, 145.16, 144.66, 144.62, 144.41, 144.35, 143.16, 143.02, 142.68, 142.63, 142.58, 142.18, 142.16, 142.09, 142.04, 142.02, 141.95, 141.82, 141.75, 141.55, 140.21, 140.04, 139.39, 136.70, 136.35, 135.70, 135.32, 135.26, 133.56 (C-16′), 76.10 (C-2), 75.90 ($Csp^3$-$C_{60}$), 74.77 (C-3), 69.93 (C-5), 69.70 ($Csp^3$-$C_{60}$), 61.42 ($CH_2$), 54.93 (C-14′), 54.37 (C-9′), 48.83 (C-13′), 44.58 (C-5′), 41.96 ($CH_2$), 40.82 ($CH_3$-N), 36.23 (C-1′), 35.65 (C-10′), 33.74 (C-8′), 33.60 (C-4′), 34.17 (C-12′), 32.06 (C-15′), 31.14 (C-7′), 28.19 (C-6′), 27.14 (C-2′), 20.65 (C-11′), 15.51 ($CH_3$-C-13′), 14.07 ($CH_3$), 12.14 ($CH_3$-C-10′). IR ($CHCl_3$): $\nu$ 2924, 2856, 2791, 1736, 1217, 1027, 771 $cm^{-1}$. UV−vis: $\lambda_{max}$ (log $\varepsilon$) 434 (3.56), 342 (4.30) 312 (4.55) nm. HRMS-MALDI-TOF: $[M + H]^+$ $m/z$ calcd for $C_{87}H_{41}ClNO_4$ 1198.2724, found 1198.2718.

*N-Methyl-(2S)-[3′β-(61″-(ethoxycarbonyl)-61″-(3′β-O-carbethoxy)methane [60]Fullerene)-17′-chloro-5α-androstan-16′-ene]pyrrolidino[3,4:1,2][60]fullerene (**6**).* A solution of $C_{60}$ (30 mg, 0.042 mmol) in toluene (50 mL) was prepared. *N*-Methyl-(2*S*)-(3′β-ethylmalonate-17′-chloro-5α-androstan-16′-ene pyrrolidino[3,4:1,2]-[60]fullerene (**5**) (50 mg, 0.042 mmol), $CBr_4$ (14 mg, 0.042 mmol), and diazabicyclo[4.2.0]undec-7-ene (DBU, 0.08 mL, 0.53 mmol) were added in that order. The reaction mixture was then stirred at room temperature for 4 h. Water was then added, and the residue was extracted with toluene. The combined extracts were dried with $MgSO_4$ and filtered, and the solvent was removed under reduced pressure. Purification of the product was achieved by column chromatography on silica gel, first with $CS_2$ to elute unreacted $C_{60}$ and dichloromethane/hexane (4:1) to elute the corresponding fullerene dumbbell **6**, yield of isolate pure product 43 mg (0.023 mmol, 55%), amorphous brown solid. HPLC: toluene/acetonitrile (9:1), flow rate 1 mL/min, $t_R$ = 10.3 min. $[\alpha]^{20}_D$ = +25 ($c$, 2 × $10^{-4}$ $CH_2Cl_2$). $^1$H NMR (700 MHz, $CDCl_3$, 25 °C): $\delta$ 5.13 (m, 1H, 3′-H), 5.02 (br s, 1 H, 2-H), 4.89 (br s, 1 H, 5-H), 4.48 (q, $^3J_{HH}$ = 14.3 Hz, $^3J_{HH}$ = 7.2 Hz, 2 H, $CH_2$), 4.05 (br s, 1 H, 5-H), 2.83 (br. s., 4 H, $CH_3$-N and 15′-H), 2.42 (m, 1 H, 15′-H), 2.00 (m, 1 H, 2′-H), 1.83 (m, 1 H, 1′-H), 1.75 (m, 1 H, 12′-H), 1.72 (m, 1 H, 7′-H), 1.66 (m, 1 H, 2′-H), 1.60 (m, 3 H, 4′-H, 8′-H, 11′-H), 1.50 (m, 2 H, 1′-H, 6′-H), 1.37 (m, 1 H, 11′-H), 1.32 (m, 1 H, 4′-H), 1.30 (m, 1 H, 14′-H), 1.31 (t, $^3J_{HH}$ = 7.2 Hz, 3 H, $CH_3$), 1.20 (m, 2 H, 5′-H, 12′-H), 1.08 (s, 3 H, $CH_3$-C-13′), 0.88 (s, 3 H, $CH_3$-C-10′), 0.75 (m, 1 H, 7′-H), 0.69 (m, 1 H, 9′-H). $^{13}$C NMR (175 MHz, $CDCl_3$, 25 °C): $\delta$ 164.02 (C═O), 163.50 (C═O), 155.91, 154.09, 153.91, 152.84, 147.33, 147.28, 146.68 146.55 (C-17′), 146.39, 146.30, 146.19, 146.09, 146.05, 146.01, 145.97, 145.77, 145.56, 145.49, 145.44, 145.39, 145.37, 145.35, 145.30, 145.28, 145.26, 145.25, 145.23, 145.20, 145.19 145.16, 145.16, 144.91, 140.71, 144.66, 144.62, 144.41, 144.35, 143.90, 143.16, 143.10, 143.02, 142.68, 142.63, 142.58, 142.18, 142.16, 142.09, 142.04, 142.02, 141.96, 141.95, 141.82, 141.75, 141.55, 140.98, 140.21, 140.04, 139.62, 139.39, 139.02, 136.70, 136.35, 135.70, 135.32, 135.26, 133.52 (C-16′), 76.11 (C-2), 75.92 ($Csp^3$-$C_{60}$), 74.30 ($Csp^3$ cyclopropane ring), 74.17 (C-3′), 71.22 ($Csp^3$ cyclopropane ring), 69.92 (C-5), 69.73 ($Csp^3$-$C_{60}$), 54.27 (C-9′), 52.93 (C-14′), 50.12 ($Csp^3$ cyclopropane ring), 48.63 (C-13′), 44.68 (C-5′), 42.01 ($CH_2$), 40.81 ($CH_3$-N), 36.18 (C-1′), 35.74 (C-10′), 34.15 (C-12′), 33.60 (C-4′), 33.51 (C-8′), 31.02 (C-15′), 30.81 (C-7′), 28.20 (C-6′), 27.14 (C-2′), 20.62 (C-11′), 15.66 ($CH_3$), 14.11 ($CH_3$-C-13′), 12.24 ($CH_3$-C-10′). IR ($CHCl_3$): $\nu$ 2923, 2854, 1740, 1681, 1457, 1238, 752, 708 $cm^{-1}$. UV−vis: $\lambda_{max}$ (log $\varepsilon$) 430 (3.27), 330 (4.60) nm. HRMS-MALDI-TOF: $[M + H]^+$ $m/z$ calcd for $C_{147}H_{39}ClNO_4$ 1916.2562, found 1916.2642. MS-MALDI (DCTB, NaI): $[M + Na]^+$ $m/z$ $C_{147}H_{38}ClNNaO_4$ 1938.

## ■ ASSOCIATED CONTENT

### Ⓢ Supporting Information

Spectra of all compounds, HPLC chromatograms of the reaction mixtures and pure products, absolute configuration assignement, and complementary theoretical data. This material is available free of charge via the Internet at http://pubs.acs.org.

## ■ AUTHOR INFORMATION


### Corresponding Authors

*E-mail: msuarez@fq.uh.cu.

*E-mail: nazmar@quim.ucm.es.


### Notes

The authors declare no competing financial interest.

## ■ ACKNOWLEDGMENTS

Financial support by the Ministerio de Economía y Competitividad (MINECO) of Spain (projects CTQ2010-16959; Consolider-Ingenio CSD2007-00010), the CAM (MADRISOLAR-2 project S2009/PPQ-1533), is acknowledged. M.S. is indebted to Programa del Grupo Santander 2012. We also want to acknowledge Prof. Hans Mikosch from Technical University of Viena for helpful discussions.

## REFERENCES


(1) (a) Nierengarten, J:-F.; Iehl, J.; Oerthel, V.; Holler, M.; Illescas, B. M.; Muñoz, A.; Martín, N.; Rojo, J.; Sánchez-Navarro, M.; Cecioni, S.; Vidal, S.; Buffet, K.; Durka, M.; Vincent, S. P. *Chem. Commun.* **2010**, *46*, 3860−3862. (b) Compain, P.; Decroocq, C.; Iehl, J.; Holler, M.; Hazelard, D.; Mena-Barragán, T.; Ortiz Mellet, C.; Nierengarten, J.-F. *Angew. Chem.* **2010**, *49*, 5753−5756. (c) Sánchez-Navarro, M.; Muñoz, A.; Illescas, B. M.; Rojo, J.; Martín, N. *Chem.—Eur. J.* **2011**, *17*, 766−769. (d) Cecioni, S.; Oerthel, V.; Iehl, J.; Holler, M.; Goyard, D.; Praly, J.-P.; Imberty, A.; Nierengarten, J.-F.; Vidal, S. *Chem.—Eur. J.* **2011**, *17*, 3252−3261. (e) Durka, M.; Buffet, K.; Iehl, J.; Holler, M.; Nierengarten, J.-F.; Taganna, J.; Bouckaert, J.; Vincent, S. P. *Chem. Commun.* **2011**, *47*, 1321−1323. (f) Durka, M.; Buffet, K.; Iehl, J.; Holler, M.; Nierengarten, J.-F.; Vincent, S. P. *Chem.—Eur. J.* **2012**, *18*, 641−651. (g) Rísquez-Cuadro, R.; García-Fernández, J. M.; Nierengarten, J.-F.; Ortiz-Mellet, C. *Chem.—Eur. J.* **2013**, *19*, 16791−16803. (h) Luczkowiak, J.; Muñoz, A.; Sánchez-Navarro, M.; Ribeiro-Viana, R.; Ginieis, A.; Illescas, B. M.; Martín, N.; Delgado, R.; Rojo, J. *Biomacromolecules* **2013**, *14*, 431−437.

(2) Mehta, G.; Goverdhan, S. V. *Chem. Soc. Rev.* **2002**, *31*, 324−334.

(3) (a) Ali, S. S.; Hardt, J. I.; Quick, K. L.; Kim-Han, J. S.; Erlanger, B. F.; Huang, T. T.; Epsrein, C. J.; Dugan, L. L. *Free Radical Med.* **2004**, *37*, 1191−1202. (b) Tzirakis, M. D.; Orfanopoulos, M. *Chem. Rev.* **2013**, *113*, 5262−5321.

(4) Bjelakovic, M. S.; Godjevac, D. M.; Milic, D. R. *Carbon* **2007**, *45*, 2260−2265.

(5) Li, L. S.; Hu, Y. J.; Wu, Y.; Wu, Y. L.; Yue, J.; Yang, F. *J. Chem. Soc., Perkin Trans. 1* **2001**, 617−621.

(6) MacFarland, D.; Zhang, J.; Zhou, Z.; Lenk, R. P.; Wilson, S. R. U. S. Pat. Appl. Publ. US 2008214514 A1 20080904, 2008.

(7) Ishi-I, T.; Shinkai, S. *Tetrahedron* **1999**, *55*, 12515−12530.

(8) Coro, J.; Rodríguez, H.; Rivera, D. G.; Suárez, M.; Molero, D.; Herranz, M. A.; Martínez-Álvarez, R.; Filippone, S.; Martín, N. *Eur. J. Org. Chem.* **2009**, 4810−4817.

(9) Ruiz, A.; Coro, J.; Almagro, L.; Ruiz, J. A.; Molero, D.; Maroto, E. E.; Filippone, S.; Herranz, M. A.; Martínez-Alvarez, R.; Sancho-García, J. C.; Di Meo, F.; Suárez, M.; Martín, N. *J. Org. Chem.* **2013**, *78*, 2819−2826.

(10) (a) Wang, Y.; Wang, Y. K.; Wang, J. M.; Liu, Y.; Yang, Y. T. *J. Am. Chem. Soc.* **2009**, *131*, 8839−8845. (b) Autschbach, J.; Nitsh-Velasquez, L.; Rudolph, M. *Top. Curr. Chem.* **2011**, *298*, 1−98. (c) Autschbach, J. *Chirality* **2009**, *21*, E116−E152. (d) McCann, D. M.; Stephens, P. J. *J. Org. Chem.* **2006**, *71*, 6074−6098. (e) Lunazzi, L.; Mancinelli, M.; Mazzanti, A.; Pierini, M. *J. Org. Chem.* **2010**, *75*, 5927−5933. (f) Dai, J.; Krohn, K.; Elsasser, B.; Florke, U.; Draeger, S.; Schulz, B.; Pescitelli, B.; Salvadori, P.; Antus, S.; Kurtan, T. *Eur. J. Org. Chem.* **2007**, *72*, 4845−4866. (g) Pescitelli, G.; Sreerama, N.; Salvadori, P.; Nakanishi, K.; Berova, N.; Woody, R. W. *J. Am. Chem. Soc.* **2008**, *130*, 6170−6179. (h) Talotta, C.; Gaeta, C.; Troisi, F.; Monaco, G.; Zanasi, R.; Mazzeo, G.; Rosini, C.; Placido, N. *Org. Lett.* **2010**, *12*, 2912−2915. (i) Jorge, F. E.; Autschbach, J.; Ziegler, T. *J. Am. Chem. Soc.* **2005**, *127*, 975−985. (j) Autschbach, J. *Chirality* **2010**, *21*, S116−S152.

(11) Toivonen, T. L.; Hukka, T. I.; Cramariuc, O.; Rantala, T. T.; Lemmetyinen, H. *J. Phys. Chem. A* **2006**, *110*, 12213−12221.

(12) Yamada, M.; Rivera-Fuentes, P.; Schweizer, W. B.; Diederich, F. *Angew. Chem., Int. Ed.* **2010**, *49*, 3532−3535.

(13) Kumar, K. S.; Patnaik, A. *J. Comput. Chem.* **2010**, *31*, 1182−1194.

(14) (a) Furche, F.; Ahlrichs, R. *J. Am. Chem. Soc.* **2002**, *124*, 3804−3805. (b) Furche, F.; Ahlrichsa, R. *J. Chem. Phys.* **2001**, *114*, 10362−10367.

(15) Yang, G.; Si, Y.; Su, Z. *J. Phys. Chem. A* **2011**, *115*, 13356−13363.

(16) (a) Maggini, M.; Scorrano, G.; Prato, M. *J. Am. Chem. Soc.* **1993**, *115*, 9798−9799. (b) Prato, M.; Maggini, M. *Acc. Chem. Res.* **1998**, *31*, 519−526.

(17) (a) Hirsch, A. *The Chemistry of Fullerenes*; Wiley-VCH: Weinheim, Germany, 2005. (b) *Fullerenes: From Synthesis to Optoelectronic Properties*; Guldi, D. M., Martín, N., Eds.; Kluwer Academic Publishers: Dordrecht, The Netherlands, 2002. (c) Taylor, R. *Lecture Notes on Fullerene Chemistry: A Handbook for Chemists*; Imperial College Press: London, 1999.

(18) Maroto, E. E.; Filippone, S.; Martín-Domenech, A.; Suárez, M.; Martín, N.; Martínez-Álvarez, R. *J. Mass. Spectrom.* **2011**, *46*, 1016−1029.

(19) Cardullo, F.; Seiler, P.; Isaacs, L.; Nierengarten, J. F.; Haldimann, R. E.; Diederich, F.; Mordasini-Denti, T.; Thiel, W.; Boudon, C.; Gisselbrecht, J. P.; Gross, M. *Helv. Chim. Acta* **1997**, *80*, 343−371.

(20) Filippone, S.; Maroto, E. E.; Martín-Domenech, A.; Suárez, M.; Martín, N. *Nat. Chem.* **2009**, *1*, 578−582.

(21) Maroto, E. E.; de Cozar, A.; Filippone, S.; Martín-Domenech, A.; Suárez, M.; Cossío, F. P.; Martín, N. *Angew. Chem., Int. Ed.* **2011**, *50*, 6060−6064.

(22) (a) Maroto, E. E.; de Cozar, A.; Filippone, S.; Martín-Domenech, A.; Suárez, M.; Cossío, F. P.; Martín, N. *J. Am. Chem. Soc.* **2012**, *134*, 12936−12938. (b) Maroto, E. E.; Filippone, S.; Suárez, M.; Martínez-Álvarez, R.; de Cózar, A.; Cossío, F. P.; Martín, N. *J. Am. Chem. Soc.* **2014**, *136*, 705−712.

(23) Dewar, M. J. S.; Zoebisch, E. G.; Healy, E. F.; Stewart, J. P. *J. Am. Chem. Soc.* **1985**, *107*, 3902−3909.

(24) Desiraju, G. R. *Acc. Chem. Res.* **2002**, *35*, 565−573.

(25) Thallapally, P. K.; Nangia, A. *CrystEngComm* **2001**, *27*, 1−6.

(26) (a) Martin, N.; Perez, I.; Sanchez, L.; Seoane, C. *J. Org. Chem.* **1997**, *22*, 5690−5695. (b) Suárez, M.; Verdecia, Y.; Illescas, B.; Martinez-Alvarez, R.; Alvarez, A.; Ochoa, E.; Seoane, C.; Kayali, N.; Martin, N. *Tetrahedron* **2003**, *59*, 9179−9186. (c) Illescas, B. M.; Martín, N.; Poater, J.; Solá, M.; Aguado, G. P.; Artuño, R. M. *J. Org. Chem.* **2005**, *70*, 6929−6932. (d) Van der Pol, C.; Bryce, M. R.; Wielopolski, M.; Atienza-Castellanos, C.; Guldi, D. M.; Filippone, S.; Martin, N. *J. Org. Chem.* **2007**, *72*, 6662−6671.

(27) Ajamaa, F.; Figueira Duarte, T. M.; Bourgogne, C.; Holler, M.; Fowler, P. W.; Nierengarten, J.-F. *Eur. J. Org. Chem.* **2005**, 3766−3774.

(28) Klamt, A.; Schuurmann, G. *J. Chem. Soc., Perkin Trans. 2* **1993**, 799−805.

(29) Barone, V.; Cossi, M. *J. Phys.Chem. A* **1998**, *102*, 1995−2001.

(30) Cossi, M.; Rega, N.; Scalmani, G.; Barone, V. *J. Comput. Chem.* **2002**, *24*, 669−681.

(31) Orlandi, G.; Negri, F. *Photochem. Photobiol. Sci.* **2002**, *1*, 289−308.

(32) Kuwahara, S.; Obata, K.; Yoshida, K.; Matsumoto, T.; Harada, N.; Yasuda, N.; Ozawa, Y.; Toriumi, K. *Angew. Chem.* **2005**, *117*, 2302−2305.

(33) Autschbach, J.; Nitsch-Velasquez, L.; Rudolph, M. *Top Curr. Chem.* **2011**, *298*, 1−98.

(34) Dreuw, A.; Head-Gordon, M. *Chem. Rev.* **2005**, *105*, 4009−4037.

(35) For comparison of theoretical and experimental circular dichroism spectra it is a common practice to fit the position of an individual Cotton effect found in the theoretical spectrum to the experimental one. This is performed by scaling the theoretical transitions by a factor that is the ratio between the theoretical and experimental Cotton effect. This methodology is widely used for comparing theoretical and experimental spectra. See for instance: (a) Diedrich, C.; Grimme, S. *J. Phys. Chem. A.* **2003**, *107*, 2524−2539. (b) Gawronski, J. K.; Kwit, M.; Boyd, D. R.; Sharma, N. D.; Malone, J. F.; Drake, A. F. *J. Am. Chem. Soc.* **2005**, *127*, 4308−4319.3. (c) Yamada, M.; Rivera-Fuentes, P.; Schweizer, W. B.; Diederich, F. *Angew. Chem., Int. Ed.* **2010**, *49*, 3532−3535. (d) Autschbach, J.; Nitsh-Velasquez, L.; Rudolph, M. *Top. Curr. Chem.* **2011**, *298*, 1−98. (e) Pikulska, A.; Hopmann, K. H.; Bloino, J.; Pecul, M. *J. Phys. Chem. B* **2013**, *117*, 5136−5147.4.

(36) Montero, L. A.; Esteva, A. M.; Molina, J.; Zapardiel, A.; Hernández, L.; Márquez, H.; Acosta, A. *J. Am. Chem. Soc.* **1998**, *120*, 12023−12033.

(37) Perez-Labrada, K.; Brouard, I.; Morera, C.; Estevez, F.; Bermejo, J.; Rivera, D. G. *Tetrahedron* **2011**, *67*, 7713−7727.

(38) Becke, A. D. *J. Chem. Phys.* **1992**, *96*, 2155−2160.
(39) Runge, E.; Gross, E. K. E. *Phys. Rev. Lett.* **1984**, *52*, 997−1000.
(40) Stephens, P. J.; Harada, N. *Chitality* **2010**, *22*, 229−233.